INTERNATIONAL JOURNAL FOR NUMERICAL AND ANALYTICAL METHODS IN GEOMECHANICS
Int. J. Numer. Anal. Meth. Geomech. 2008; **32**:833–861
Published online 16 July 2007 in Wiley InterScience (www.interscience.wiley.com). DOI: 10.1002/nag.648

A model for stress and plastic strain induced nonlinear, hyperelastic anisotropy in soils

A. Gajo and D. Bigoni*, †

Dipartimento di Ingegneria Meccanica e Strutturale, Università di Trento, Via Mesiano 77, I-38050 Povo, Trento, Italy

SUMMARY

The experimental evidence that cohesive and granular soils possess an elastic range in which the elasticity is both nonlinear and anisotropic—with stiffness and directional characteristics strongly dependent on stress and plastic strain (the so-called 'stress history')—is given a formulation based on hyperelasticity. This is accomplished within the framework of elastoplastic coupling, through a new proposal of elastic potentials and a combined use of a plastic-strain-dependent fabric tensor and nonlinear elasticity. When used within a simple elastoplastic framework, the proposed model is shown to yield very accurate simulations of the evolution of elastic properties from initial directional stiffening to final isotropic degradation. Within the proposed constitutive framework, it is shown that predictions of shear band formation and evolution become closer to the existing experimental results, when compared to modelling in which elasticity does not evolve. Copyright © 2007 John Wiley & Sons, Ltd.

Received 2 November 2006; Revised 21 May 2007; Accepted 21 May 2007

KEY WORDS: elastic behaviour; anisotropy; sand; clay; shear bands; elastoplasticity

Dedicated to Prof. Tomasz Hueckel on the occasion of his 60th birthday

1. INTRODUCTION

Experimental evidence shows that deformation of cohesive and granular soils at very small strains (less than about 0.001% for sands and 0.01% for clays) is essentially recoverable and rate insensitive [1–7]. While in this range of strains the elastic response is very stiff, at larger strain, when irreversible deformations become important, two concurrent phenomena occur, namely, a decrease of tangential stiffness and a degradation of elastic moduli (an experimental evidence recently

*Correspondence to: D. Bigoni, Dipartimento di Ingegneria Meccanica e Strutturale, Università di Trento, Via Mesiano 77, I-38050 Trento, Italy.
†E-mail: bigoni@ing.unitn.it, URL: http://www.ing.unitn.it/~bigoni

Contract/grant sponsor: MURST-Cofin 2005; contract/grant number: 2005085973_002

provided by Kuwano and Jardine [8], and Hoque and Tatsuoka [9]). In other words, the elastic behaviour is highly nonlinear and plastic strain dependent. In addition, the elasticity exhibits important directional properties evolving with both the stress and the plastic strain states. In summary, elasticity of soils depends on (Appendix A):

- the void ratio,
- the stress state,
- the so-called 'stress history', which is here modelled in terms of plastic strain.

All the above dependencies regard both the elastic stiffness and the elastic anisotropy. In particular, the anisotropy, which is usually a class of orthotropy,[‡] may be *inherent*, thus resulting from soil deposition, and *induced* by stress and/or plastic strain.

The understanding of the above-described elastic behaviour of soil—having both theoretical importance (since it proves that soils exhibit an elastic range, the fundamental starting point for plasticity theory) and practical relevance for design of geotechnical structures—is deemed by Atkinson [15] as 'one of the major achievements of geotechnical engineering research over the past 30 years'. Accordingly, a strong research effort has been devoted to constitutive description of the elastic properties of soils. In particular,[§] the *stress dependence* of elastic moduli and the *stress-induced* elastic cross anisotropy have been modelled by Vermeer [17], Boyce [18], Mroz and Norris [19], Loret [20], Houlsby [21], Jardine *et al*. [22], Lade and Nelson [23], Molekamp [24], Puzrin and Burland [25] and Houlsby *et al*. [26] for clay and sand, while the only attempt to describe *plastically induced* anisotropy is due to Hueckel *et al*. [27], for overconsolidated clays.[¶] Modelling of *both stress and plastic* dependency of elasticity has never been attempted.

A comprehensive model capable of describing the evolution of stress and plastically induced (hyper-)elastic anisotropy, including the dependence of elastic stiffness on the stress, void ratio and plastic states and the stiffness degradation occurring at large applied shear stress is still lacking. Such a constitutive model is formulated in this article and it is shown to agree with available experimental results.

In particular, a new nonlinear hyperelastic model is introduced (in Sections 2 and 3), which can describe a general evolution of elastic anisotropy and the stress dependency of elastic properties. This model is developed within the framework of elastoplastic coupling [30–33], in which the elastic anisotropy is induced partly by the stress state and partly by the plastic strain state, through the definition of a fabric tensor [34, 35]. Elastic orthotropy with rotating axes can be described, together with the stress and the density dependency of elastic stiffness and its degradation at large stress ratio, observed in recent experiments by Hoque and Tatsuoka [9]. Due to the double source

[‡]For orthotropy, a convenient measure of the anisotropy degree is the ratio between elastic Young's moduli in the horizontal and vertical directions $n = E_h/E_v$. In normally consolidated clays, this ratio n may range between 0.9 and 1.35 [10, 11]. In heavily overconsolidated clays, a much larger anisotropy can be observed with typical values of n ranging between 1.35 and 2.4 [12, 13]. Finally in sands, n can vary from 0.9 to 0.64 in a triaxial compression test performed in a subangular sand, and from 0.9 to 1.23 in a triaxial extension test [14]. For subrounded sands subjected to triaxial compression n can be smaller than 0.35 [9].

[§]We do not consider here hypoelastic models, for which residual elastic strain and energy may be extracted from closed stress and strain paths, respectively [16].

[¶]An alternative to phenomenological modelling of granular material is the micromechanical approach, pursued, among others, by Walton [28] and Goddard [29]. However, the lack of a self-adjointed structure of governing equations, as related to the presence of Coulomb friction, hampers the development of micromechanical modelling, which remains for the moment limited to simple situations.

DOI: 10.1002/nag

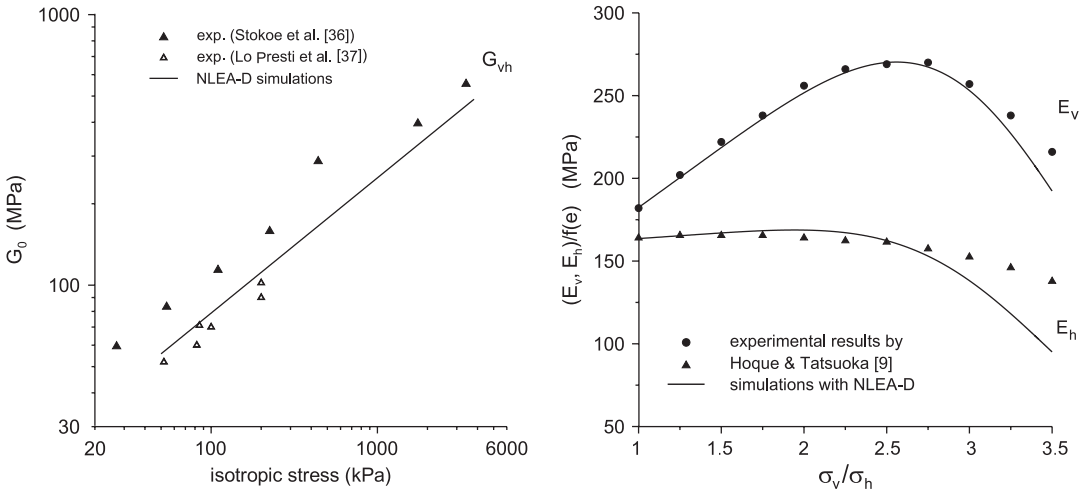

Figure 1. Comparison between simulations (obtained for dense Hostun sand with $e_0 = 0.673$) and experimental results concerning: (left) the variation of small-strain shear modulus measured on samples subjected to increasing isotropic confining pressure (experimental results of Stokoe *et al*. [36] and Lo Presti *et al*. [37]); (right) the evolution of small-strain vertical and horizontal Young's moduli measured on a sample subjected to increasing vertical stress at constant horizontal stress in a triaxial cell (experimental results taken from Hoque and Tatsuoka [9]).

of elastic anisotropy, namely plastic strain and stress state, experimental results pertaining to sand can be appropriately simulated (and we believe that incorporation of the behaviour of clay would not be difficult).

The introduced hyperelastic model is general, so that the typical ingredients of plasticity theory (yield surface, hardening function, and flow rule) are left unspecified. However, we incorporate (in Section 4) the proposed model of anisotropy into a standard isotropic-hardening-based constitutive framework. In particular, granular materials are addressed, so that the flow rule is borrowed from the Cam Clay model, a yield surface with a smooth Mohr–Coulomb-like shape is used, in which the angular opening is taken to be dependent on the accumulated deviatoric plastic strains (in this way a smooth stress–strain behaviour is simulated) and on the state parameter ψ (describing the dependence of strength on density and stress level). Within this simple constitutive framework, we analyse (in Section 5) different anisotropy models at increasing levels of sophistication (and complexity) by simulating representative triaxial and plane strain tests.

The capability of the proposed models of hyperelasticity implemented in a simple elastoplasticity framework to simulate a wide range of experimentally observed properties is summarized in Figure 1 on the left, where the consistency of the simulated mean-stress dependency of elastic stiffness in a isotropic compression test is shown. The capability of simulated evolution of elastic stiffness anisotropy and elastic stiffness degradation occurring in triaxial compression at stress ratios larger than about $\sigma_v/\sigma_h > 2.5$ is shown in Figure 1, on the right.

Finally, the effects of the new constitutive formulation on the initiation and development of shear bands are presented in Section 6, where it is shown that the nonlinear elastic anisotropy model gives results that are almost coincident with those obtained with a linear elastic anisotropy model. Moreover, important differences of response are obtained when elastic stiffness degradation

DOI: 10.1002/nag

is taken into account, together with the very high initial stiffness typically observed in soils at very small strains. However, the experimental results that are currently available in the regime of substantial strain in triaxial and biaxial tests do not permit a proper model calibration, so that our work will hopefully stimulate further experimental investigation, concerning in particular the phenomenon of elastic degradation.

2. THE CONCEPT OF ELASTOPLASTIC COUPLING

The evolution of elastic anisotropy and the elastic stiffness degradation with the accumulation of plastic strain (namely, the permanent deformation obtained after complete unloading) can be described within the framework of elastic–plastic coupling [30–33, 38].

We begin postulating that the effective stress $\boldsymbol{\sigma}$ (or the elastic strain, $\boldsymbol{\varepsilon}_e$) is a prescribed function of the plastic deformation $\boldsymbol{\varepsilon}_p$, and the elastic strain (or the effective stress, $\boldsymbol{\sigma}$), namely

$$\boldsymbol{\sigma} = \hat{\boldsymbol{\sigma}}(\boldsymbol{\varepsilon}_p, \boldsymbol{\varepsilon}_e), \quad \boldsymbol{\varepsilon}_e = \hat{\boldsymbol{\varepsilon}}_e(\boldsymbol{\varepsilon}_p, \boldsymbol{\sigma}) \tag{1}$$

where the elastic and plastic strains are defined only upon total unloading, so that they obey the additive strain decomposition

$$\boldsymbol{\varepsilon} = \boldsymbol{\varepsilon}_e + \boldsymbol{\varepsilon}_p \tag{2}$$

Taking the rate of Equations (1) and using the rate form of Equation (2) we obtain

$$\dot{\boldsymbol{\sigma}} = \frac{\partial \hat{\boldsymbol{\sigma}}}{\partial \boldsymbol{\varepsilon}_e}[\dot{\boldsymbol{\varepsilon}}] - \left(\frac{\partial \hat{\boldsymbol{\sigma}}}{\partial \boldsymbol{\varepsilon}_e} - \frac{\partial \hat{\boldsymbol{\sigma}}}{\partial \boldsymbol{\varepsilon}_p}\right)[\dot{\boldsymbol{\varepsilon}}_p], \quad \dot{\boldsymbol{\varepsilon}} = \frac{\partial \hat{\boldsymbol{\varepsilon}}_e}{\partial \boldsymbol{\sigma}}[\dot{\boldsymbol{\sigma}}] + \left(\frac{\partial \hat{\boldsymbol{\varepsilon}}_e}{\partial \boldsymbol{\varepsilon}_p} + \mathbb{S}\right)[\dot{\boldsymbol{\varepsilon}}_p] \tag{3}$$

where $\mathbb{S}$ is the symmetrizing fourth-order tensor, which singles out the symmetric part of every second-order tensor $\mathbf{X}$

$$\mathbb{S}[\mathbf{X}] = \tfrac{1}{2}(\mathbf{X} + \mathbf{X}^T) \tag{4}$$

Before continuing, two observations are necessary.

- First, note that a substitution of Equation $(1)_1$ in Equation $(1)_2$ yields the condition

$$\boldsymbol{\varepsilon}_e = \hat{\boldsymbol{\varepsilon}}_e(\boldsymbol{\varepsilon}_p, \hat{\boldsymbol{\sigma}}(\boldsymbol{\varepsilon}_p, \boldsymbol{\varepsilon}_e)) \tag{5}$$

  which, differentiated with respect to $\boldsymbol{\varepsilon}_e$ and $\boldsymbol{\varepsilon}_p$, and using the chain rule, gives

$$\frac{\partial \hat{\boldsymbol{\varepsilon}}_e}{\partial \hat{\boldsymbol{\sigma}}} \frac{\partial \hat{\boldsymbol{\sigma}}}{\partial \boldsymbol{\varepsilon}_e} = \mathbb{S}, \quad \frac{\partial \hat{\boldsymbol{\varepsilon}}_e}{\partial \boldsymbol{\varepsilon}_p} = -\frac{\partial \hat{\boldsymbol{\varepsilon}}_e}{\partial \hat{\boldsymbol{\sigma}}} \frac{\partial \hat{\boldsymbol{\sigma}}}{\partial \boldsymbol{\varepsilon}_p} \tag{6}$$

  showing that two expressions $(3)_1$ and $(3)_2$ are equivalent.
- Second, let us consider a small stress cycle of loading and unloading from a state defined by $\{\boldsymbol{\sigma}, \boldsymbol{\varepsilon}_p\}$, in which the stress is first incremented and subsequently decremented by $\Delta\boldsymbol{\sigma}$ (Figure 2), thus producing an increment $\Delta\boldsymbol{\varepsilon}_p$ in the plastic deformation. Expanding

DOI: 10.1002/nag

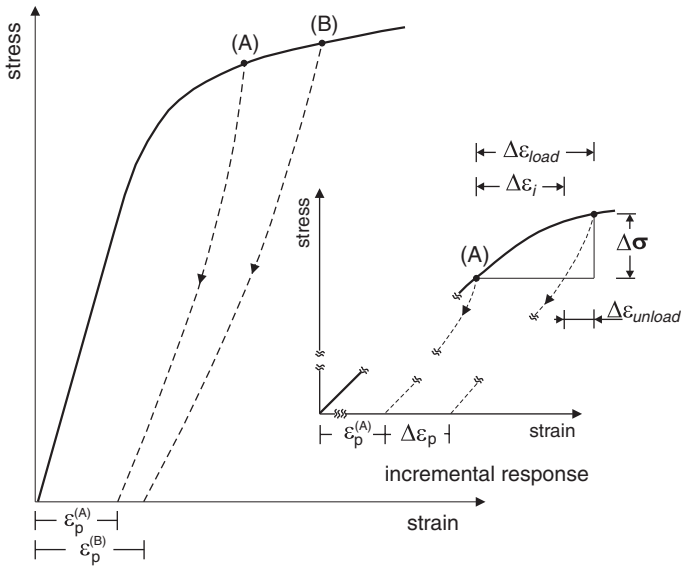

Figure 2. Elastoplastic coupling with a nonlinear elastic law.

Equation $(1)_2$ for loading and unloading we get, respectively:

$$\Delta\boldsymbol{\varepsilon}_{\text{load}} = \left.\frac{\partial\hat{\boldsymbol{\varepsilon}}_{\text{e}}}{\partial\boldsymbol{\sigma}}\right|_{\{\boldsymbol{\sigma},\boldsymbol{\varepsilon}_{\text{p}}\}} [\Delta\boldsymbol{\sigma}] + \left(\left.\frac{\partial\hat{\boldsymbol{\varepsilon}}_{\text{e}}}{\partial\boldsymbol{\varepsilon}_{\text{p}}}\right|_{\{\boldsymbol{\sigma},\boldsymbol{\varepsilon}_{\text{p}}\}} + \mathbb{S}\right)[\Delta\boldsymbol{\varepsilon}_{\text{p}}] + O\left(\Delta\boldsymbol{\sigma}^2, \Delta\boldsymbol{\varepsilon}_{\text{p}}^2\right)$$

$$\Delta\boldsymbol{\varepsilon}_{\text{unload}} = \left.\frac{\partial\hat{\boldsymbol{\varepsilon}}_{\text{e}}}{\partial\boldsymbol{\sigma}}\right|_{\{\boldsymbol{\sigma}+\Delta\boldsymbol{\sigma},\boldsymbol{\varepsilon}_{\text{p}}+\Delta\boldsymbol{\varepsilon}_{\text{p}}\}} [-\Delta\boldsymbol{\sigma}] + O(\Delta\boldsymbol{\sigma}^2)$$

$$= \left.\frac{\partial\hat{\boldsymbol{\varepsilon}}_{\text{e}}}{\partial\boldsymbol{\sigma}}\right|_{\{\boldsymbol{\sigma},\boldsymbol{\varepsilon}_{\text{p}}\}} [-\Delta\boldsymbol{\sigma}] + O(\Delta\boldsymbol{\sigma}^2, \Delta\boldsymbol{\varepsilon}_{\text{p}}^2) \tag{7}$$

showing that for an infinitesimal loading/unloading cycle, the irreversible strain rate $\dot{\boldsymbol{\varepsilon}}_{\text{i}}$ differs from the plastic strain rate $\dot{\boldsymbol{\varepsilon}}_{\text{p}}$ and follows the rule:

$$\dot{\boldsymbol{\varepsilon}}_{\text{i}} = \mathbb{G}[\dot{\boldsymbol{\varepsilon}}_{\text{p}}] \tag{8}$$

where

$$\mathbb{G} = \mathbb{S} - \mathbb{D}^{-1}\frac{\partial\hat{\boldsymbol{\sigma}}}{\partial\boldsymbol{\varepsilon}_{\text{p}}} = \mathbb{S} + \frac{\partial\hat{\boldsymbol{\varepsilon}}_{\text{e}}}{\partial\boldsymbol{\varepsilon}_{\text{p}}} \tag{9}$$

in which tensor $\mathbb{D}$ is defined as [keeping into account Equation (6)]

$$\mathbb{D} = \frac{\partial\hat{\boldsymbol{\sigma}}}{\partial\boldsymbol{\varepsilon}_{\text{e}}} = \left(\frac{\partial\hat{\boldsymbol{\varepsilon}}_{\text{e}}}{\partial\boldsymbol{\sigma}}\right)^{-1} \tag{10}$$

DOI: 10.1002/nag

Going back now to Equations (3) and following Hill and Rice [38] and Bigoni [39], we can introduce the flow rule, defining the rate of irreversible strain as

$$\dot{\boldsymbol{\varepsilon}}_{\mathrm{i}} = \dot{\lambda}\mathbf{P} \tag{11}$$

where $\mathbf{P}$ defines the 'direction' of the irreversible strain rate and $\dot{\lambda} \geqslant 0$ its modulus, so that $\dot{\lambda} = 0$ for unloading.

Assuming now the existence of a yield function (discriminating between elastic and inelastic states)

$$f(\boldsymbol{\sigma}, \mathscr{K}) \leqslant 0 \tag{12}$$

where $\mathscr{K}$ represents a *generic set* of hidden variables, Prager's consistency yields

$$\mathbf{Q} \cdot \dot{\boldsymbol{\sigma}} = H\dot{\lambda} \tag{13}$$

where

$$\mathbf{Q} = \frac{\partial f}{\partial \boldsymbol{\sigma}} \tag{14}$$

is the yield function gradient and

$$H\dot{\lambda} = -\frac{\partial f}{\partial \mathscr{K}} \cdot \dot{\mathscr{K}} \tag{15}$$

in which H is the plastic modulus, positive (negative) for strain hardening (softening) and null for perfectly plastic behaviour.

Using now Equations (11) and (13) with $(3)_1$, we obtain

$$\dot{\lambda} = \frac{\langle \mathbf{Q} \cdot \dot{\boldsymbol{\sigma}} \rangle}{H} \tag{16}$$

valid for $H > 0$ and

$$\dot{\lambda} = \frac{\langle \mathbf{Q} \cdot \mathbb{D}[\dot{\boldsymbol{\varepsilon}}] \rangle}{H + \mathbf{Q} \cdot \mathbb{D}[\mathbf{P}]} \tag{17}$$

valid for $H + \mathbf{Q} \cdot \mathbb{D}[\mathbf{P}] > 0$, where the Macaulay bracket operator is defined for every $\alpha \in \Re$ as $\langle \alpha \rangle = (\alpha + |\alpha|)/2$.

The rate equations are obtained in the form

$$\dot{\boldsymbol{\varepsilon}} = \mathbb{D}^{-1}[\dot{\boldsymbol{\sigma}}] + \frac{\langle \mathbf{Q} \cdot \dot{\boldsymbol{\sigma}} \rangle}{H}\mathbf{P} \tag{18}$$

$$\dot{\boldsymbol{\sigma}} = \mathbb{D}[\dot{\boldsymbol{\varepsilon}}] - \frac{\langle \mathbf{Q} \cdot \mathbb{D}[\dot{\boldsymbol{\varepsilon}}] \rangle}{H + \mathbf{Q} \cdot \mathbb{D}[\mathbf{P}]}\mathbb{D}[\mathbf{P}] \tag{19}$$

Equations (18) and (19) describe elastoplastic coupling with nonlinear elasticity and have been introduced in full generality. The formulation is so general that even the existence of a free-energy density is, strictly speaking, not needed. Since the importance of introducing a hyperelastic law is

DOI: 10.1002/nag

well known, it is expedient to operate now with a free-energy density $\varphi(\boldsymbol{\varepsilon}_p, \boldsymbol{\varepsilon}_e)$ or a complementary free-energy density $\psi(\boldsymbol{\varepsilon}_p, \boldsymbol{\sigma})$, so that Equations (1) are obtained as

$$\boldsymbol{\sigma} = \frac{\partial \varphi\left(\boldsymbol{\varepsilon}_p, \boldsymbol{\varepsilon}_e\right)}{\partial \boldsymbol{\varepsilon}_e}, \quad \boldsymbol{\varepsilon}_e = \frac{\partial \psi\left(\boldsymbol{\varepsilon}_p, \boldsymbol{\sigma}\right)}{\partial \boldsymbol{\sigma}} \tag{20}$$

At this point, to obtain a model describing the small-strain mechanical behaviour of soils we need to prescribe:

- a form for the free-energy density φ (or the complementary free-energy density ψ), incorporating:
  - a nonlinear dependence on elastic strain (or stress in a representation based on complementary free-energy) reproducing: (i) the mean-stress dependence of the elastic tangent stiffness (Equation (40)) and (ii) the stress-induced elastic anisotropy,
  - a second-order fabric tensor depending on deviatoric plastic strain reproducing the fraction of plastically induced elastic anisotropy,
  - a scalar dependence on plastic strain describing the elastic degradation and void-ratio dependency [9].
- a plastic constitutive framework, incorporating:
  - a yield function (either reproducing the mean stress and density dependence of shear strength for granular materials, or the effects of stress history for clays),
  - a flow rule (reproducing the observed irreversible dilatancy),
  - a hardening rule (reproducing the progressive decrease of stiffness typical of soils).

A free-energy density satisfying the above-mentioned requisites is provided in the Section 3 (and a generalization of it, plus an alternative version of complementary free-energy density is given in Appendix B), while the plastic framework is briefly presented in Section 4.

3. THE PLASTIC STRAIN-DEPENDENT, NONLINEAR FREE-ENERGY DENSITY

The free-energy density function φ is proposed in the form

$$\varphi(\boldsymbol{\varepsilon}_e, \boldsymbol{\varepsilon}_p) = \alpha d(-\mathrm{tr}(\mathbf{B}\boldsymbol{\varepsilon}_e))^n + \beta d(\mathrm{tr}(\mathbf{B}\boldsymbol{\varepsilon}_e)^2)^l \tag{21}$$

where $\mathbf{B}$ is a symmetric, second-order, positive-definite fabric tensor, subject to the constraint

$$\mathrm{tr}\,\mathbf{B}^2 = 3 \tag{22}$$

describing fabric anisotropy and depending on the plastic strain $\boldsymbol{\varepsilon}_p$ [34, 35, 40], α, β, l, and n are material parameters and $d = d(\boldsymbol{\varepsilon}_p)$ is a function of the plastic strain introduced to describe the elastic stiffness degradation and void-ratio dependency (that will be specified later).

When elastic stiffness degradation and void-ratio dependency are neglected (i.e. d is constant) and, moreover, $n = 2$ and $l = 1$, the linear elastic anisotropy inspired by Valanis [34] and Bigoni and Loret [35] is recovered, so that when $\mathbf{B} = \mathbf{I}$, linear isotropic elasticity is eventually recovered.

DOI: 10.1002/nag

From the elastic potential (21), the stress $\boldsymbol{\sigma}$ can be immediately derived

$$\boldsymbol{\sigma} = \frac{\partial \varphi}{\partial \boldsymbol{\varepsilon}_e} = -\alpha d n(-\mathrm{tr}(\mathbf{B}\boldsymbol{\varepsilon}_e))^{n-1}\mathbf{B} + 2\beta d l(\mathrm{tr}(\mathbf{B}\boldsymbol{\varepsilon}_e)^2)^{l-1}\mathbf{B}\boldsymbol{\varepsilon}_e\mathbf{B} \tag{23}$$

Equivalently, the stress increment $\dot{\boldsymbol{\sigma}}$ can be obtained by taking the rates of Equation (23)

$$\dot{\boldsymbol{\sigma}} = \mathbb{D}[\dot{\boldsymbol{\varepsilon}}_e] + \frac{\partial^2 \varphi}{\partial \boldsymbol{\varepsilon}_e \partial \mathbf{B}}[\dot{\mathbf{B}}] + \frac{\partial^2 \varphi}{\partial \boldsymbol{\varepsilon}_e \partial d}\left(\frac{\partial d}{\partial \boldsymbol{\varepsilon}_p} \cdot \dot{\boldsymbol{\varepsilon}}_p\right) \tag{24}$$

where

$$\dot{\mathbf{B}} = \frac{\partial \mathbf{B}}{\partial \boldsymbol{\varepsilon}_p}[\dot{\boldsymbol{\varepsilon}}_p] \tag{25}$$

The tangent elastic stiffness $\mathbb{D}$ tensors appearing in Equation (24) is

$$\mathbb{D} = k_1 \mathbf{B} \otimes \mathbf{B} + k_2 \mathbf{B}\boldsymbol{\varepsilon}_e\mathbf{B} \otimes \mathbf{B}\boldsymbol{\varepsilon}_e\mathbf{B} + k_3 \mathbf{B} \underline{\overline{\otimes}}\, \mathbf{B} \tag{26}$$

where two tensorial products have been employed, which can be defined as

$$(\mathbf{A} \otimes \mathbf{B})[\mathbf{C}] = (\mathbf{B} \cdot \mathbf{C})\mathbf{A}, \quad (\mathbf{A}\underline{\overline{\otimes}}\mathbf{B})[\mathbf{C}] = \tfrac{1}{2}(\mathbf{A}\mathbf{C}\mathbf{B}^{\mathrm{T}} + \mathbf{A}\mathbf{C}^{\mathrm{T}}\mathbf{B}^{\mathrm{T}}) \tag{27}$$

for every second-order tensor **A**, **B**, and **C** (see also Appendix C for an alternative matrix-form representation).

The fourth-order tensor describing the effects related to $\dot{\mathbf{B}}$ in Equation (24) is

$$\frac{\partial^2 \varphi}{\partial \boldsymbol{\varepsilon}_e \partial \mathbf{B}} = \widetilde{k}_1 \mathbf{B} \otimes \boldsymbol{\varepsilon}_e + \widetilde{k}_2 \mathbf{I}\underline{\overline{\otimes}}\mathbf{I} + \widetilde{k}_3 \mathbf{B}\boldsymbol{\varepsilon}_e\mathbf{B} \otimes \boldsymbol{\varepsilon}_e\mathbf{B}\boldsymbol{\varepsilon}_e + \widetilde{k}_4(\mathbf{B}\boldsymbol{\varepsilon}_e\underline{\overline{\otimes}}\mathbf{I} + \mathbf{I}\underline{\overline{\otimes}}\mathbf{B}\boldsymbol{\varepsilon}_e) \tag{28}$$

and finally the second-order tensor describing the effects induced by a rate in d in Equation (24) is

$$\frac{\partial^2 \varphi}{\partial \boldsymbol{\varepsilon}_e \partial d} = \bar{k}_1 \mathbf{B} + \bar{k}_2 \mathbf{B}\boldsymbol{\varepsilon}_e\mathbf{B} \tag{29}$$

In Equations (26) and (29), the coefficients k_i, $\widetilde{k}_i$, and $\bar{k}_i$ are functions of $\mathrm{tr}(\mathbf{B}\boldsymbol{\varepsilon}_e)$, and $\mathrm{tr}(\mathbf{B}\boldsymbol{\varepsilon}_e)^2$, reported for conciseness in Appendix D.

We finally remark that the positive definiteness of the tangent stiffness $\mathbb{D}$ tensor is important in view of the implications on material stability and is addressed in Appendix E. Sufficient conditions (these become also necessary when coefficients k_i, $i = 1, .., 3$ are constants) for positive definiteness of the fourth-order tensor $\mathbb{D}$ for every value of elastic deformation $\boldsymbol{\varepsilon}_e$ are

$$k_1 + \tfrac{1}{3}k_3 > 0, \quad k_2 > 0, \quad k_3 > 0 \tag{30}$$

The coupling fourth-order tensor $\mathbb{G}$ turns out to be

$$\mathbb{G} = \mathbb{S} - \mathbb{D}^{-1}\frac{\partial^2 \varphi}{\partial \boldsymbol{\varepsilon}_e \partial \mathbf{B}}\frac{\partial \mathbf{B}}{\partial \boldsymbol{\varepsilon}_p} - \mathbb{D}^{-1}\frac{\partial^2 \varphi}{\partial \boldsymbol{\varepsilon}_e \partial d} \otimes \frac{\partial d}{\partial \boldsymbol{\varepsilon}_p} \tag{31}$$

and it must be positive definite (for reasons detailed in Gajo *et al*. [41]), a condition that can be checked along the given stress path.

DOI: 10.1002/nag

3.1. A sensitive choice of elastic evolution laws

The elastic degradation and the void-ratio dependency are described by employing functions $d_1(\gamma^{\mathrm{p}}_{\mathrm{oct}})$ and $d_2(\mathrm{tr}\,\boldsymbol{\varepsilon}_{\mathrm{p}})$, respectively, which enter the formulation through their product

$$d(\boldsymbol{\varepsilon}_{\mathrm{p}}) = d_1(\gamma^{\mathrm{p}}_{\mathrm{oct}}) d_2(\boldsymbol{\varepsilon}_{\mathrm{p}}) = \left[1 - r\left(1 - \frac{t}{t + \gamma^{\mathrm{p}}_{\mathrm{oct}}}\right)\right]\left[\frac{(3.17 - v_0(1 + \mathrm{tr}\,\boldsymbol{\varepsilon}_{\mathrm{p}}))^2}{v_0(1 + \mathrm{tr}\,\boldsymbol{\varepsilon}_{\mathrm{p}})}\right] \tag{32}$$

where r and t are two constitutive parameters, $v_0 = 1 + e_0$ is the initial specific volume and $\gamma^{\mathrm{p}}_{\mathrm{oct}}$ is the accumulated octahedral plastic strain, namely,

$$\gamma^{\mathrm{p}}_{\mathrm{oct}} = \int_{\text{deformation path}} \sqrt{\frac{1}{3}\mathrm{dev}\,\dot{\boldsymbol{\varepsilon}}_{\mathrm{p}} \cdot \mathrm{dev}\,\dot{\boldsymbol{\varepsilon}}_{\mathrm{p}}} \tag{33}$$

Note that for null deviatoric plastic strain the elastic degradation is null, namely $d_1(0) = 1$, whereas at large deviatoric plastic strains $d_1(\infty) = 1 - r$, so that $1 - r$ represents the asymptotic value of degradation. The parameter t governs the elastic stiffness degradation rate in terms of $\gamma^{\mathrm{p}}_{\mathrm{oct}}$.

The evolution law of tensor $\mathbf{B}$ has been selected and calibrated by Gajo *et al.* [41] from experimental results; that law is now generalized to account for inherent anisotropy as follows:

$$\mathbf{B} = \mathrm{dev}\,\mathbf{B}_* + \sqrt{\frac{3 - \mathrm{dev}\,\mathbf{B}_* \cdot \mathrm{dev}\,\mathbf{B}_*}{3}}\mathbf{I} \tag{34}$$

where

$$\mathbf{B}_* = \mathbf{B}_0 - \beta\boldsymbol{\varepsilon}_{\mathrm{p}} \tag{35}$$

and $\mathbf{B}_0$ is the initial value of the fabric tensor due to soil deposition (i.e. the *inherent anisotropy* at null plastic strains), the function $\beta = \beta(J_{2\,(\varepsilon_{\mathrm{p}})}, \theta_{(\varepsilon_{\mathrm{p}})})$ depends on the plastic strain, through the second invariant

$$J_{2\,(\varepsilon_{\mathrm{p}})} = \tfrac{1}{2}\mathrm{dev}\,\boldsymbol{\varepsilon}_{\mathrm{p}} \cdot \mathrm{dev}\,\boldsymbol{\varepsilon}_{\mathrm{p}} \tag{36}$$

and the Lode angle invariant

$$\theta_{(\varepsilon_{\mathrm{p}})} = \frac{1}{3}\cos^{-1}\left(\frac{3\sqrt{3}}{2}\frac{J_{3\,(\varepsilon_{\mathrm{p}})}}{J^{3/2}_{2\,(\varepsilon_{\mathrm{p}})}}\right) \tag{37}$$

of the plastic strain, according to

$$\beta(J_{2\,(\varepsilon_{\mathrm{p}})}, \theta_{(\varepsilon_{\mathrm{p}})}) = \frac{A_\varepsilon g(\theta_{(\varepsilon_{\mathrm{p}})})}{B_\varepsilon g(\theta_{(\varepsilon_{\mathrm{p}})}) + \sqrt{2J_{2\,(\varepsilon_{\mathrm{p}})}}} \tag{38}$$

with

$$g(\theta_{(\varepsilon_{\mathrm{p}})}) = \frac{2m_\varepsilon}{1 + m_\varepsilon + (1 - m_\varepsilon)\cos 3\theta_{(\varepsilon_{\mathrm{p}})}} \tag{39}$$

DOI: 10.1002/nag

and A_ε, B_ε, and m_ε are non-negative constitutive parameters. In Equation (38) a hyperbolic relationship is introduced between the deviatoric component of $\mathbf{B}$ and the deviatoric component of $\boldsymbol{\varepsilon}_\mathrm{p}$. At zero deviatoric plastic strain, the plastically induced anisotropy is zero and the fabric tensor is related only to *inherent anisotropy* through $\mathbf{B}=\mathbf{B}_0$ (usually not much different from the identity tensor), whereas at very large deviatoric plastic strains, the fabric tensor $\mathbf{B}$ reaches a saturation condition. Elastic isotropy is recovered when $A_\varepsilon=0$ (in this case the elasto-plastic coupling disappears) and $\mathbf{B}=\mathbf{B}_0=\mathbf{I}$.

Note that Equation (39) is tailored to capture the behaviour of sands, since the stiffness increases in the direction of major principal compressive plastic strain. Different from sand and due to the specific shape of the particles, the elastic anisotropy decreases for clays in the direction of major principal compressive plastic strain [42]. This behaviour could be modelled by replacing for instance $\mathbf{B}$ with $\mathbf{B}^{-1}$ in Equation (34).

Due to our isotropic hardening assumption, Equations (32) and (34) are appropriate only for describing elastic stiffness degradation and evolution in a monotonic loading test (since d and $\mathbf{B}$ remain 'frozen' upon unloading). The experimental fact that elastic anisotropy also changes along unloading paths [8] requires introduction of kinematic hardening and is not pursued here for simplicity.

3.2. Calibration of elasticity parameters

The elastic behaviour is described by providing the evolution of the fabric tensor $\mathbf{B}$, Equation (34), and the elastic stiffness, Equation (32). The calibration of the fabric tensor has been detailed in Gajo *et al*. [41]. The inherent anisotropy, represented by the second-order tensor $\mathbf{B}_0$, is calibrated from the experimental data given by Hoque and Tatsuoka [9]. The parameters used in the simulations are presented in Table I.

In order to calibrate parameters α, β, n, and l, we refer to the following general law to describe the evolution of elastic stiffness of sands in terms of specific volume ($v_0=1+e_0$) and mean effective pressure (p):

$$\mu_0 = g_1 p_\mathrm{r} \frac{(g_2 - v_0)^2}{v_0} \left(\frac{p}{p_\mathrm{r}}\right)^{0.5} \tag{40}$$

Table I. Values of soil parameters for describing the evolution of the fabric tensor of Hostun sand RF, valid for all our models, except the values marked with (*) which refer to the NLEA-D model (see Equation (43)).

Parameter	Description	Values
A_ε	Parameter controlling the asymptotic value of the fabric tensor in uniaxial compression	1.35
B_ε	Parameter controlling the hyperbolic evolution of the fabric tensor with plastic strain	0.02, 0.40(*)
m_ε	Parameter controlling the asymptotic value of the fabric tensor in uniaxial extension	0.45
$(\mathbf{B}_0)_{11}$	Inherent anisotropy in the vertical direction	1.044183
$(\mathbf{B}_0)_{22}=(\mathbf{B}_0)_{33}$	Inherent anisotropy in the horizontal direction	0.977159
$(\mathbf{B}_0)_{ij}, i\neq j$	Inherent anisotropy in transverse direction	0.000000

DOI: 10.1002/nag

(where $p_r = 1\,\text{kPa}$ is a reference pressure) and we use two sets of parameters g_1 and g_2, namely,

- $g_1 = 3230$ and $g_2 = 3.97$, as suggested by Hardin and Richart [43] and representing a reasonably simple estimate in the absence of *ad hoc* experiments (used by Gajo and Muir Wood [44, 45] and Gajo *et al.* [41])
- $g_1 = 7730$ and $g_2 = 3.17$, which were calibrated by Hoque and Tatsuoka [9] on the experimental results (on Toyura sand) that will be used later to test the validity of our constitutive modelling.[‖]

The calibration of the elasticity parameters α, β, n, and l has been obtained by observing that with null fabric anisotropy (i.e. $\mathbf{B} = \mathbf{I}$) and isotropic stress state (i.e. $\boldsymbol{\sigma} = -p\mathbf{I}$), the tangent elastic stiffness tensor, Equation (26), reduces to an isotropic (nonlinear) elastic law. Therefore, the coefficients have been calibrated by imposing that under such conditions the tangent stiffness strictly obeys Equation (40), thus reproducing the observed proportionality of the tangent stiffness to the square root of mean stress.

In the following, three particularizations of the proposed elasticity models are considered:

- The linear elastic anisotropy model adopted by Gajo *et al.* [41], labelled 'LEA', defined by:
  - Constant tangent elastic stiffness ($n = 2$ and $l = 1$) with evolving fabric tensor $\mathbf{B}$. The elastic stiffness is defined by the elastic shear modulus and Poisson's ratio, ν. The latter is taken equal to 0.1, while the former remains defined in terms of

$$\begin{aligned} \alpha &= \frac{2\nu}{(1-2\nu)}\beta \\ \beta &= \left(3230\, p_r \frac{(3.97-\bar{v})^2}{\bar{v}}\right)\left(\frac{\bar{p}}{p_r}\right)^{0.5} \end{aligned} \tag{41}$$

    where $\bar{p}$ and $\bar{v}$ are the (constant) mean effective pressure and specific volume, selected as mean values referred to the considered experiments.
  - Null elastic stiffness degradation ($r = 0.80$ and $t = 0$, thus $d_1(\gamma^{\text{p}}_{\text{oct}}) = 0.20$).
  - Null specific volume dependency of elastic stiffness ($d_2(\boldsymbol{\varepsilon}_{\text{p}}) = 1$).
- A nonlinear elastic anisotropy model, labelled 'NLEA', defined as 'LEA' except that:
  - A stress-dependent tangent elastic stiffness is introduced ($n = 3$ and $l = 1.5$), with evolving fabric tensor $\mathbf{B}$. Constants α and β become

$$\begin{aligned} \alpha &= \frac{5\nu - 1}{6\sqrt{3}(1-2\nu)}\beta \\ \beta &= \frac{2(1+\nu)}{3\sqrt{3}(1-2\nu)}\left(3230\, p_r \frac{(3.97-\bar{v})^2}{\bar{v}}\right)^2 \end{aligned} \tag{42}$$

    with $\nu = 0.1$.

[‖]For dense sand ($e = 0.60$), the two sets of parameters in Equation (40) produce a difference in terms of μ_0 of about 5%, whereas for loose sand ($e = 0.90$) the difference is about 10%.

DOI: 10.1002/nag

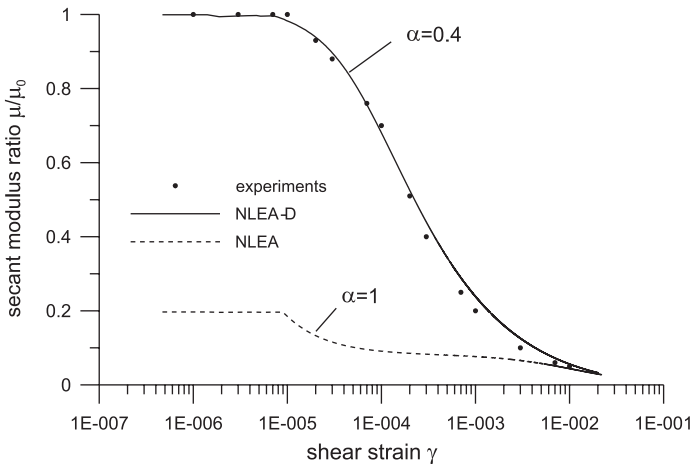

Figure 3. Evolution of the apparent secant shear stiffness ratio μ/μ_0 measured in torsional shear tests on Ticino sand (experimental results from Lancellotta and Calavera [48]) and simulated as a simple shear test at the mean initial pressure of $p_0 = 100\,\text{kPa}$ on dense Hostun sand ($e_0 = 0.673$). The corresponding evolution of elastic anisotropy is given in Figure 7.

- A nonlinear elastic anisotropy model with elastic stiffness degradation and void-ratio dependency of elastic stiffness, labelled 'NLEA-D', defined as 'NLEA' except that:
  - Constants α and β calibrated on experimental results by Kuwano and Jardine [8] and Hoque and Tatsuoka [9] on Toyura sand

$$\alpha = \frac{5\nu - 1}{6\sqrt{3}(1-2\nu)}\beta$$
$$\beta = \frac{2(1+\nu)}{3\sqrt{3}(1-2\nu)}(7730 p_r)^2 \tag{43}$$

    with $\nu = 0.1$.
  - Elastic stiffness degradation ($r = 0.80$ and $t = 0.0001$).
  - Specific volume dependency of elastic stiffness, Equation (32).

As a simple particularization of the LEA model, we will refer sometimes in the following to the linear isotropic elasticity, labelled 'LEI' (obtained by setting $A_\varepsilon = 0$ and $\mathbf{B}_0 = \mathbf{I}$, so that $\mathbf{B} = \mathbf{I}$).

It is important to emphasize that elastic anisotropy is entirely induced by plastic strains in the LEA model, through the evolution of the fabric tensor $\mathbf{B}$, while elastic anisotropy is induced partly by plastic strain and partly by stress in the NLEA and NLEA-D models. Under isotropic stress conditions, with null fabric anisotropy (i.e. $\mathbf{B} = \mathbf{I}$), both NLEA and NLEA-D models reproduce the observed proportionality of the tangent elastic stiffness on the square root of the mean pressure (Figure 1, left).

Note that the elastic stiffness in LEA and the initial elastic stiffness in NLEA are equal to $\frac{1}{5}$ of the small-strain stiffness μ_0 evaluated from empirical correlations (as assumed also by Gajo *et al.* [41]), as can be seen also in Figure 3. In NLEA-D model, in which elastic stiffness degradation is included, the initial elastic stiffness coincides with the initial small-strain stiffness μ_0, which has

DOI: 10.1002/nag

been calibrated from the small-strain measurements by Kuwano and Jardine [8] and Hoque and Tatsuoka [9] on Toyura sand.

Finally for the NLEA and NLEA-D models, the sufficient conditions $(30)_2$ and $(30)_3$ for positive definiteness of $\mathbb{D}$ are always satisfied, whereas the condition $(30)_1$ is always satisfied for $v \leqslant 2/7$ (a condition that is verified in our simulations), otherwise it is satisfied only under certain restrictions on $\mathrm{tr}(\mathbf{B}\boldsymbol{\varepsilon}_e)$.

4. A SIMPLE ELASTOPLASTIC CONSTITUTIVE FRAMEWORK INCORPORATING THE ANISOTROPIC EVOLUTION LAWS

A constitutive framework for stress and plastic strain-dependent elasticity for soils has been presented in Section 2. The formulation is very general and different choices of constitutive parameters are to be defined. The validity of our approach is tested in this section for granular materials, by introducing elastic evolutions laws at different degrees of sophistication within a simple elastoplastic model, capable of describing the behaviour of non-cohesive soils under monotonic loading. It will be shown that the performances of our elastic evolution laws is excellent.

4.1. Yield function

The (isotropic) yield function is assumed to depend on the set of internal variables γ^p_{oct} (Equation (33)) and $\mathrm{tr}\,\boldsymbol{\varepsilon}_p$ and stress $\boldsymbol{\sigma}$ as

$$f(\boldsymbol{\sigma}, \gamma^p_{oct}, \mathrm{tr}\,\boldsymbol{\varepsilon}_p) = \sqrt{J_{2(\sigma)}} - (1 - k\psi) g(\theta_{(\sigma)}) M s(\gamma^p_{oct}) p \tag{44}$$

where k is a positive constitutive parameter and the dependence on $\mathrm{tr}\,\boldsymbol{\varepsilon}_p$ is implicit in the state parameter ψ, proposed by Been and Jefferies [46] as

$$\psi = v - v_\Lambda + \Lambda \ln p \tag{45}$$

representing a 'volumetric' measure of the distance of the current state from the critical state line, corresponding to $\psi = 0$. The function $g(\theta_{(\sigma)})$ describing the deviatoric section of the yield surface is assumed in the form proposed by Argyris *et al*. [47] (where $m > 0$ is a constitutive parameter)

$$g(\theta_{(\sigma)}) = \frac{2m}{1 + m + (1 - m)\cos 3\theta_{(\sigma)}} \tag{46}$$

which is believed to provide a good match to experimental results. Finally, the function $s(\gamma^p_{oct})$ is used to describe the smooth decrease of stiffness with progressive deformation, typical of granular material, through the following hyperbolic relationship, which is inspired by an equivalent function defined by Gajo and Muir Wood [44, 45]

$$s(\gamma^p_{oct}) = \left[1 - \frac{B}{B/(1 - R^{1/\alpha}) + (\gamma^p_{oct})}\right]^\alpha \tag{47}$$

where $R < 1$, B and α are constitutive parameters, the former of which represents a measure of the initial size of the yield surface with respect to the size of the yield surface when the material reaches the peak strength, whereas B and α define the stiffness of the plastic response. Note that $s(0) = R$ when $\gamma^p_{oct} = 0$, whereas $s(\infty) = 1$ when $\gamma^p_{oct} = \infty$. Comparing Equation (47) with the

DOI: 10.1002/nag

analogous Equation (14) of Gajo *et al*. [41], we note the presence of the new parameter α, which has been introduced for improving model simulations when elastic stiffness degradation is taken into account.

4.2. Flow rule

For simplicity we use deviatoric associativity and, following Gajo and Muir Wood [44], we assume

$$\frac{\operatorname{tr}\mathbf{P}}{\|\operatorname{dev}\mathbf{P}\|} = -\sqrt{3}A\left[(1+k_{\mathrm{d}}\psi)\,M - \frac{\sqrt{J_{2\,(\varepsilon_{\mathrm{p}})}}}{g(\theta_{(\varepsilon_{\mathrm{p}})})p}\right] \tag{48}$$

where A and k_{d} are constitutive parameters. Due to deviatoric associativity, Equation (48) completely defines the tensor $\mathbf{P}$.

4.3. Hardening rule

On the basis of the assumed yield function, the following hardening rule is selected:

$$H = -v_0\frac{\partial f}{\partial \psi}\mathbf{I}\cdot\mathbb{G}^{-1}[\mathbf{P}] - \frac{1}{\sqrt{3}}\frac{\partial f}{\partial \gamma^{\mathrm{p}}_{\mathrm{oct}}}\|\operatorname{dev}\mathbb{G}^{-1}[\mathbf{P}]\| \tag{49}$$

where H is the plastic modulus, depending on the current state through $\boldsymbol{\sigma}$ and $\boldsymbol{\varepsilon}_{\mathrm{p}}$.

4.4. Calibration of the parameters describing the irreversible behaviour

Eight constitutive parameters have been introduced by Gajo *et al*. [41] to describe inelastic behaviour of sands. Now these parameters become nine, since the additional parameter α in Equation (47) has been added for defining the hardening rule. The calibration of the eight parameters for Hostun sand RF is discussed in detail elsewhere [41, 44, 45] and will not be repeated here (see Table II for a summary). As far as the calibration of the parameter α is concerned,

Table II. Values of soil parameters for describing the irreversible behaviour of Hostun sand RF, valid for all our models, except the values marked with (*) which refer to the NLEA-D model.

Parameter	Description	
v_Λ	Intercept for critical-state line in v–ln p plane at $p = 1$ kPa	1.969
Λ	Slope of critical-state line in v–ln p plane	0.030
ϕ_{cv}	Critical-state angle of friction	32°
m	Parameter controlling the deviatoric section of the yield surface	0.8
k	Link between changes in state parameter and current size of the yield surface	2.5
A	Multiplier in flow rule	0.6
k_{d}	State parameter contribution in flow rule	2.2
B	Parameter controlling hyperbolic stiffness relationship	0.004, 0.008(*)
α	Exponent controlling hyperbolic stiffness relationship	1, 0.4(*)
R	Initial size of the yield surface	0.1, 0.01(*)

DOI: 10.1002/nag

reference is made to the strong decrease of the apparent secant stiffness ratio μ/μ_0 with shear strain, which is well documented from an experimental viewpoint (e.g. Seed *et al.* [2]). In particular, the comparison between experimental results and simulations obtained with NLEA and NLEA-D models is shown in Figure 3. Here, the NLEA-D model shows its superiority with respect to the NLEA model (and equivalently also to the LEA model). In fact, only with the NLEA-D model the larger initial stiffness and the smooth decrease of apparent secant stiffness can be fairly accurately reproduced, Figure 3, through the appropriate calibration of parameters B, α, and R (denoted with an asterisk in Table II).**

Simulations of typical laboratory tests performed until substantial deformation occurred show a good agreement with available experimental data and are deferred to Appendix F.

5. RESULTS ON EVOLUTION OF ELASTIC PROPERTIES OF SAND

The evolution of directional elastic stiffness predicted by our model at different degrees of sophistication (i.e. using models LEA, NLEA, and NLEA-D) are compared with available experimental results.

The proposed nonlinear models have both a stress and a plastic strain induced elastic anisotropy. In order to evaluate the relative importance of the two contributions, simulations of a drained biaxial compression test on dense Hostun sand ($e_0 = 0.673$) at 400 kPa are considered in Figure 4. In particular, the evolution of the vertical stiffness E_v is reported on the left in Figure 4 employing the NLEA model with a varying and a fixed ($\mathbf{B} = \mathbf{B}_0$) fabric tensor. The ratio between vertical and horizontal in-plane elastic stiffnesses $E_v/E_{h,ip}$ is reported on the right in Figure 4. It can be observed that the total increase of vertical stiffness induced by both the stress and the plastic strain is very large. Moreover, it can be observed from Figure 4 (right) that the main portion of elastic anisotropy is plastic strain induced, through the evolution of the fabric tensor $\mathbf{B}$.

The complete evolution of the simulated elastic stiffness anisotropy in a drained biaxial test on dense Hostun sand ($e_0 = 0.673$) under 400 kPa of confining pressure is shown in Figure 5. The corresponding stress–strain curves are shown in Figure F2 (Appendix F).

It becomes evident from Figure 5 that the model incorporating elastic degradation (NLEA-D) has the capability of describing the very stiff initial response experimentally observed by many authors (e.g. Seed *et al.* [2]). Note, however, that there are no available experimental data on the amount of both elastic stiffness degradation and elastic anisotropy at large strains, because available measurements are limited to relatively small stress ratios ($1/3.5 \leqslant \sigma_v/\sigma_h \leqslant 3.5$ in Hoque and Tatsuoka [9]). Therefore, further experimental evaluations are needed for an appropriate calibration of the model.

The NLEA-D model simulations have been compared in Figure 6 (a part of which has been reported in Figure 1) with experimental results obtained by Hoque and Tatsuoka [9] and Kuwano and Jardine [8]. The former authors have measured local strains in drained triaxial compression and extension tests on dense Toyura sand ($e = 0.64 - 0.70$, at an initial confining pressure of 100 kPa), while the latter have used both local strain transducers and bender elements on triaxial

**The strong variation of the apparent secant stiffness has been found in our simulations to be only marginally affected by elastic degradation and to be mainly driven by plastic deformation.

DOI: 10.1002/nag

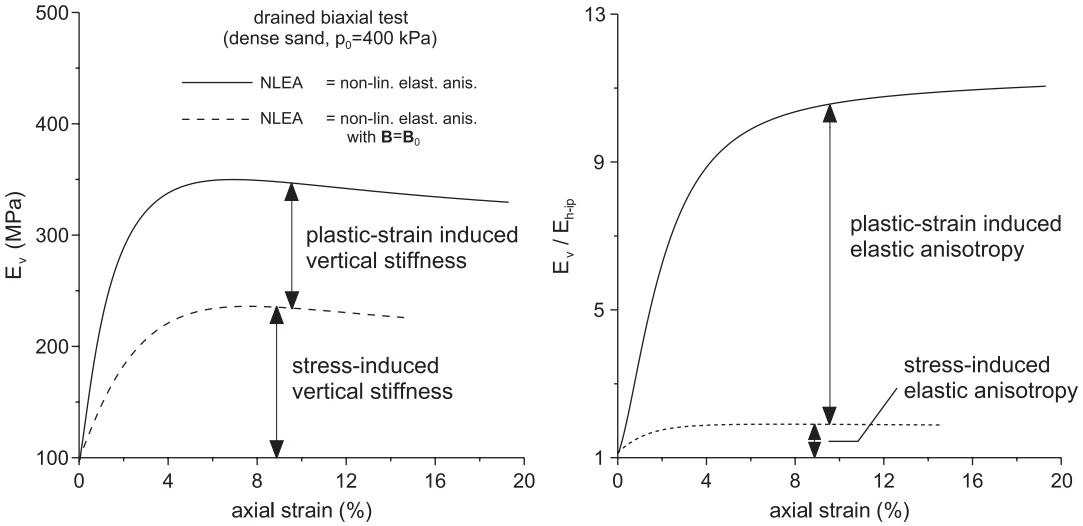

Figure 4. Comparison between different simulations of a drained biaxial compression test at the initial pressure $p_0 = 400\,\text{kPa}$ of dense Hostun sand RF ($e_0 = 0.673$). Vertical elastic stiffness E_v *versus* axial strain (left), $E_\text{v}/E_\text{h,ip}$ ratio *versus* axial strain (right).

compression samples of dense Ham River sand ($e = 0.66$, with $\sigma_\text{h}/\sigma_\text{v} = 0.45$ at an initial mean pressure ranging between 50 and 200 kPa).[††]

Note that the simulations and results reported in Figure 6 have been normalized through division by $f(e) = (2.17 - e)^2/(1 + e)$ in order to account for void-ratio variations. In the simulations, the value of Poisson's ratio was calibrated to obtain results consistent with the values of E_v and E_h measured by Hoque and Tatsuoka [9] and of G_hh and G_vh measured by Kuwano and Jardine [8]. It is clear from Figure 6 that NLEA-D simulations compare very well with measurements. In particular:

- For a compression test in which σ_h is kept constant and in the range where elastic degradation does not play an important role (i.e. for stress ratios smaller than about 2.5), E_v increases with $\sigma_\text{v}/\sigma_\text{h}$ while E_h remains roughly constant (Figure 6, left).
- For an extension test in which σ_v is kept constant and in the range where elastic degradation does not play an important role (i.e. for stress ratios smaller than about 2.5), E_h increases with $\sigma_\text{h}/\sigma_\text{v}$, while E_v remains roughly constant (Figure 6, right).
- During elastic degradation, both elastic moduli decrease with the increase of the stress ratio. Therefore, the assumed isotropic degradation law seems to be sufficiently accurate.

[††]The comparison with experimental results on Toyura and Ham River sands is motivated by the fact that to the best of authors' knowledge a similar complete set of small-strain measurements on Hostun sand is not available. Moreover, the Toyura and Ham River sands are pretty similar to Hostun sand. In fact, they are all subangular sands, with the following characteristics: $D_{50} = 0.380\,\text{mm}$, $U_\text{c} = 2$, $e_\text{max} = 1.000$, $e_\text{min} = 0.656$, for the Hostun sand $D_{50} = 0.162\,\text{mm}$, $U_\text{c} = 1.46$, $e_\text{max} = 0.973$, and $e_\text{min} = 0.612$, for the Toyura sand, and $D_{50} = 0.27\,\text{mm}$, $U_c = 1.67$, $e_\text{max} = 0.849$, $e_\text{min} = 0.547$, for the Ham River sand.

DOI: 10.1002/nag

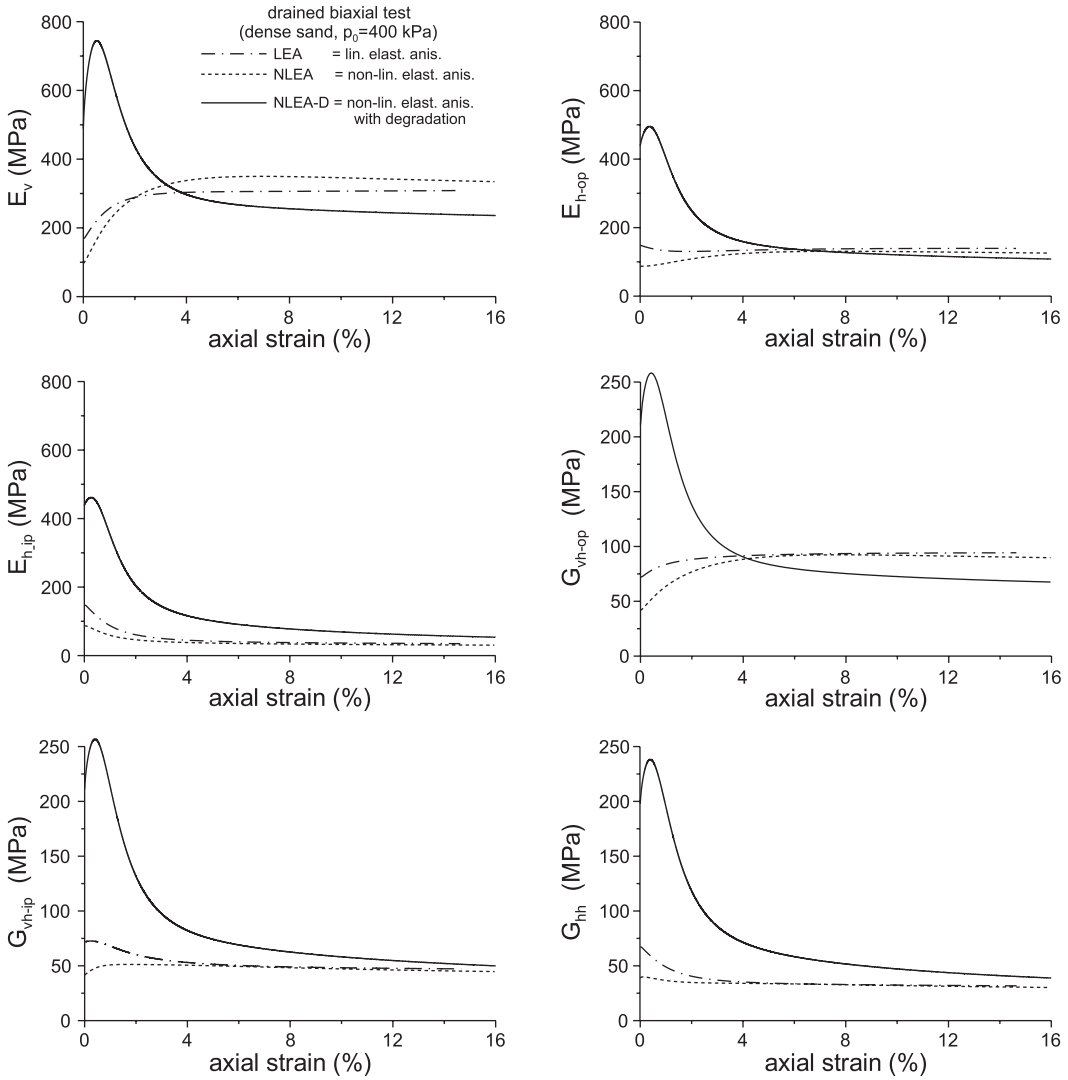

Figure 5. Evolution of the simulated elastic stiffness anisotropy in drained biaxial compression test of dense Hostun sand RF ($e_0 = 0.673$) at the initial pressure, $p_0 = 400\,\text{kPa}$.

The above reported simulations do not involve rotation of the principal stress axes. It seems now crucial to investigate the effects on the evolution of elastic properties related to such a rotation. Therefore, NLEA and NLEA-D simulations are compared in Figure 7 with experimental results obtained by HongNam and Koseki [49] on a hollow cylinder apparatus (on dense Toyura sand with initial void ratio between 0.70 and 0.74, under an initial confining pressure ranging between 30 and 400 kPa).

DOI: 10.1002/nag

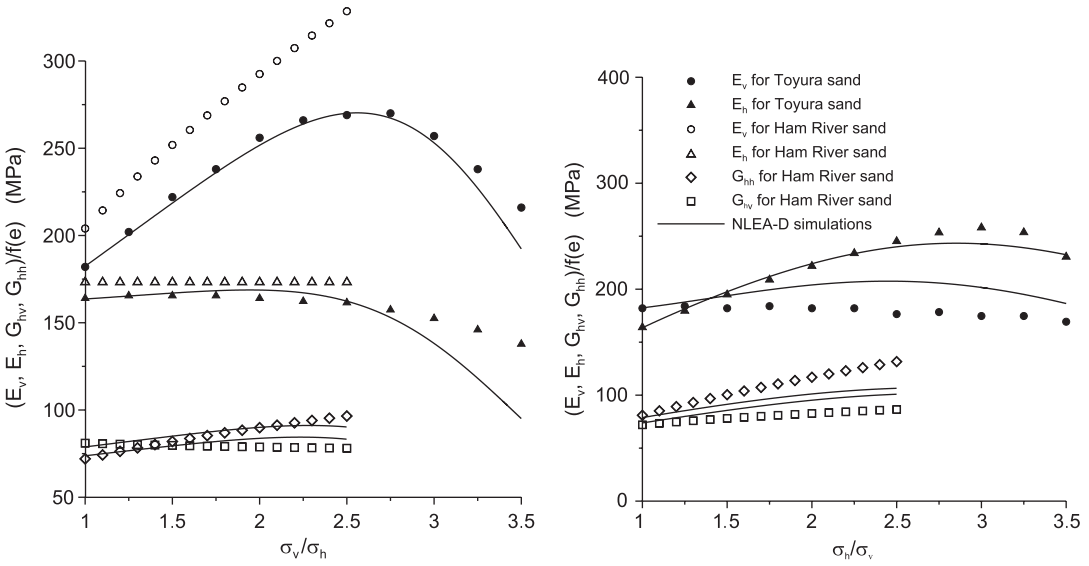

Figure 6. Comparison between measured and simulated elastic moduli in drained triaxial compression and extension tests at the initial pressure, $p_0 = 100\,\text{kPa}$ of dense Toyura sand and Ham River sand (simulated as dense Hostun sand with $e_0 = 0.673$). Compression test, where σ_h is kept constant (left); extension test, where σ_v is kept constant (right), experimental data taken from Hoque and Tatsuoka [9] and Kuwano and Jardine [8].

The comparison with NLEA and NLEA-D simulations is given in Figure 7 in terms of current elastic compliances (normalized through division by initial compliances, denoted by the index [0] in Figure 7) defined as

$$M_{11} = \frac{\dot{\varepsilon}_{zz}}{\dot{\sigma}_{zz}}, \quad M_{44} = 2\frac{\dot{\varepsilon}_{\theta z}}{\dot{\sigma}_{\theta z}}, \quad M_{14} = \frac{\dot{\varepsilon}_{zz}}{\dot{\sigma}_{\theta z}}, \quad M_{34} = \frac{\dot{\varepsilon}_{\theta\theta}}{\dot{\sigma}_{\theta z}} \tag{50}$$

(where z, r, and θ denote polar coordinates) measured along small unload/reload cycles under torsional shear.[‡‡] It can be concluded from Figure 7 that model simulations are again very consistent with the experimental evidence and that, when elastic degradation is considered (in NLEA-D model), the elastic compliance undergoes, as expected, an abrupt increase at fairly small applied shear stress.

6. CRITICAL AND POSTCRITICAL SHEAR BAND ANALYSIS

Gajo *et al.* [41, 50] have shown that elastic stiffness properties of soil play a key role on shear band nucleation and growth.[§§] They have shown that multiple shear bands may occur and that these

[‡‡] It may be interesting to note that experimental evaluations provided by HongNam and Koseki [48] refer to the elastic compliance, not to the tangent compliance. A strange aspect of these experiments is that they evidence a slightly non-symmetric elastic compliance tensor since M_{41} and M_{14} have been found to be slightly different.

[§§] The fact that elastic behaviour is important in shear banding may be easily understood when one considers that the major part of the sample is undergoing elastic unloading after strain localization.

DOI: 10.1002/nag

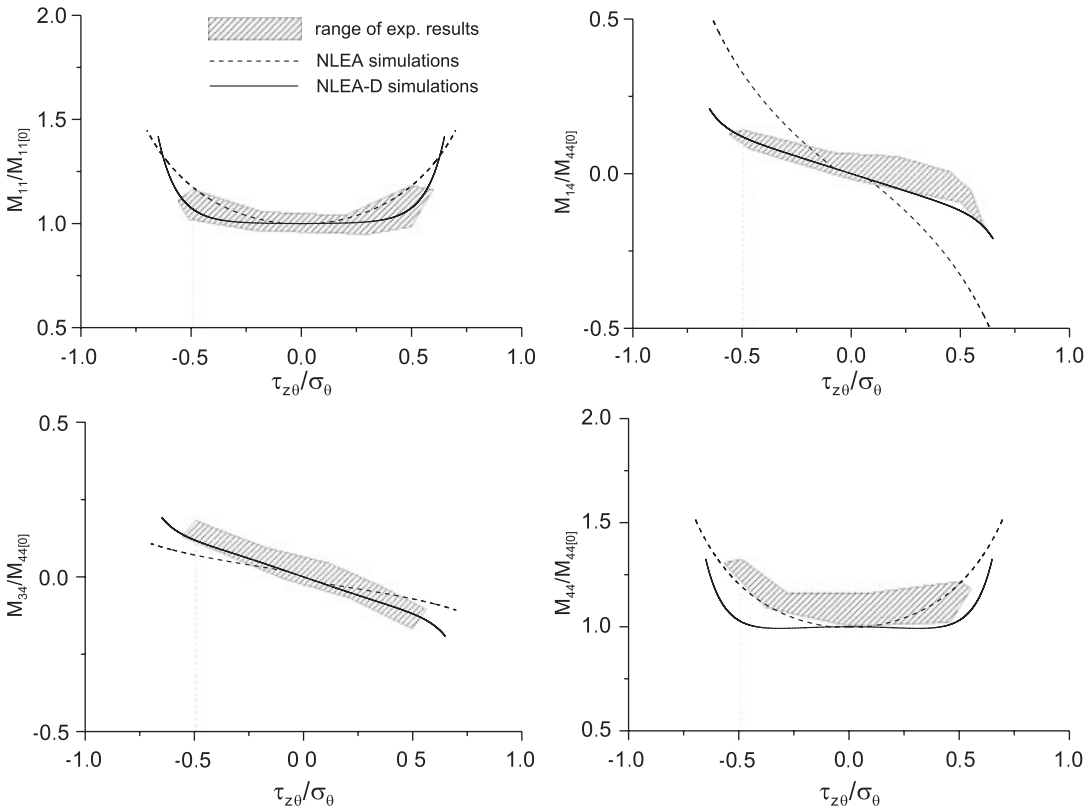

Figure 7. Comparison between measured and simulated elastic compliances in torsional shear tests performed in hollow cylinder at the mean initial pressure of $p_0 = 100$ kPa on dense Toyura sand (simulated as dense Hostun sand with $e_0 = 0.673$). Experimental data taken from [49].

may be persistent or not, depending also on the elastic properties of the material. Therefore, it is important now to investigate the effects on strain localization of the proposed constitutive model for elastic evolution (including elastic stiffening, degradation, and anisotropy reorientation).

The simulation of a drained biaxial compression test including shear band formation and growth is shown in Figure 8 for a dense Hostun sand sample ($e = 0.673$) at 400 kPa initial confining pressure. The left part of the figure refers to the models LEA, NLEA, and NLEA-D, while the effect of membrane confinement and penetration is included in the simulations on the right part obtained with the NLEA and NLEA-D models (as a reference, the curves reported in the part *a* are also included dashed). All the simulations have been performed employing the techniques explained in detail by Gajo *et al*. [41] for ideal boundary conditions (Figure 8, upper part) and by Gajo *et al*. [50] when out-of-plane compliance due to membrane penetration is included (Figure 8, lower part).

The following observations can be drawn from Figure 8.

- Results obtained with the LEA model coincide with those already reported by Gajo *et al*. ([41], their Figure 2, and [50], their Figure 8). For the values considered of density and

DOI: 10.1002/nag

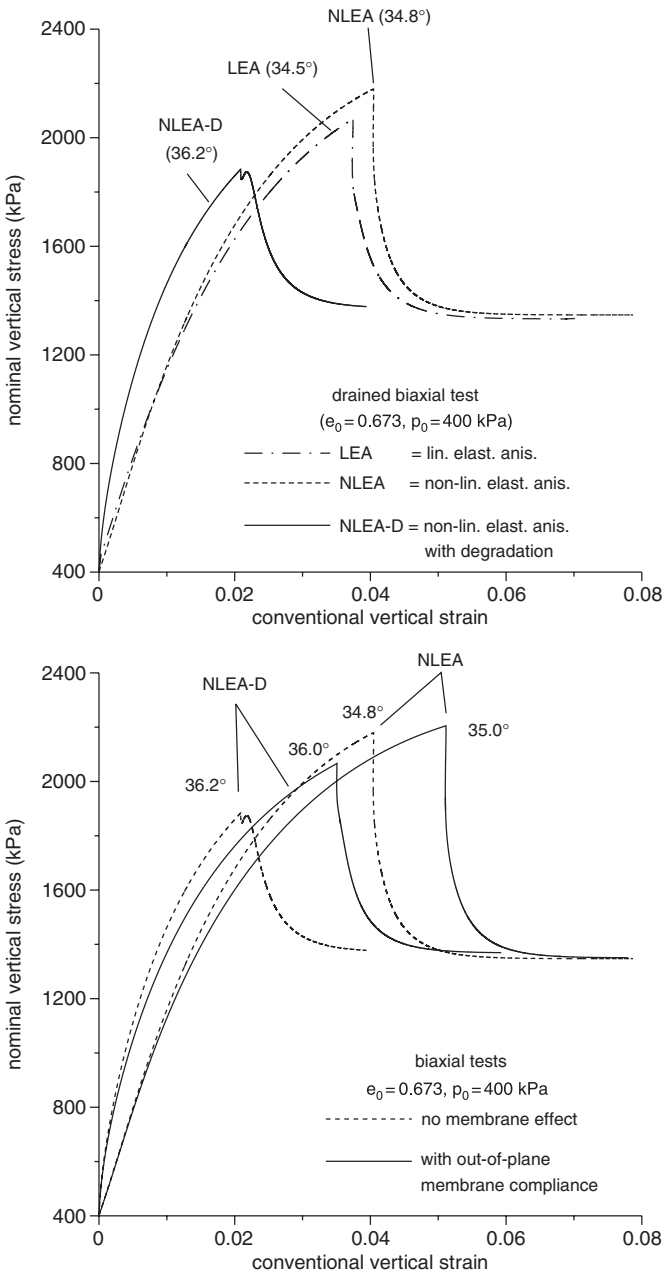

Figure 8. Simulated drained biaxial compression tests of medium dense Hostun sand ($e_0 = 0.673$) at the initial pressure of $p_0 = 400$ kPa. LEA, NLEA, and NLEA-D model simulations with perfect boundary conditions (upper part); NLEA and NLEA-D model simulations including the effects of membrane compliance (lower part); the curves on the upper part are also reported dashed on the lower part as a reference.

DOI: 10.1002/nag

confining pressure, a single shear band (inclined at 34.5° with respect to the vertical axis) forms and grows, inducing a strong softening. These results are a reference since they have been shown to be close to the available experimental results and that the agreement increases when the effects of membrane penetration are taken into account.

- Results obtained with the NLEA model are almost coincident with those obtained with the LEA model (the predicted band inclination with the former model is 34.8°).
- The simulations obtained with the NLEA-D model show that a single shear band forms, accompanied by a near-peak stress oscillation. The global behaviour is far from the simulations obtained with the other two models, a fact that is mitigated by the inclusion of membrane penetration in the analysis (Figure 8, lower part). We believe that the difference in the behaviour predicted by the NLEA-D model is due to the poor calibration of elastic degradation in the regime of substantial strain, where experimental results are currently not available (in biaxial test).

We can conclude that the NLEA model performs correctly not only in simulating homogeneous sample response, but also in predicting shear band formation and growth. On the other hand, the NLEA-D model, which does not perform correctly in the description of strain localization, deserves a more accurate calibration, based on experimental data, to be obtained from a biaxial test at substantial strain.

7. CONCLUSIONS

A new hyperelastic description of elastic stiffness and elastic anisotropy evolution in soils has been proposed (at different degrees of sophistication) within the framework of elastoplastic coupling, incorporating a law of stress-dependent, nonlinear elasticity. This represents the first attempt to describe the dependency of elastic properties of soils on both the current stress and plastic states. Equipped with a simple elastoplastic formulation, the proposed law is shown to provide an excellent description of available experimental results. The shear band formation and development analysis reveal that the proposed models provide results not far from those obtained by Gajo *et al*. [41] neglecting evolutional stiffness and stress dependency of anisotropy in the elastic description of behaviour of sand. However, differences in the results concerning localization when elastic degradation is taken into account calls for further experimental investigation.

APPENDIX A: THE EXPERIMENTAL EVIDENCE OF SMALL-STRAIN ELASTIC ANISOTROPY IN SOILS

Experimental evidence of inherent anisotropy is not firmly established for granular materials; for instance, while Stokoe *et al*. [51] and Bellotti *et al*. [52] show that the elastic Young modulus in the horizontal direction (E_h) is larger than in the vertical (E_v) for air-pluviated samples, an opposite conclusion is reached by Hoque and Tatsuoka [14] and Kuwano and Jardine [8]. In the present paper, inherent anisotropy is taken into account by introducing an initial fabric tensor $\mathbf{B}_0$ (Equation (35)), calibrated from experimental results by Hoque and Tatsuoka [9].

Concerning the induced elastic anisotropy of sands, it is generally accepted that the Young modulus in the direction of the principal stress axes is a function of the effective normal stress in

DOI: 10.1002/nag

that direction [4, 37, 53, 54] and a power law dependency is usually proposed for the vertical and horizontal directions

$$E_{\mathrm{v}} = C_{\mathrm{v}} f(v) \left(\frac{\sigma_{\mathrm{v}}}{p_{\mathrm{r}}}\right)^{a_{\mathrm{v}}}, \quad E_{\mathrm{h}} = C_{\mathrm{h}} f(v) \left(\frac{\sigma_{\mathrm{h}}}{p_{\mathrm{r}}}\right)^{a_{\mathrm{h}}} \tag{A1}$$

where C_{v} and C_{h} are two constants, the function

$$f(v) = (3.17 - v)/v \tag{A2}$$

takes into account the specific volume dependency (as suggested by Hardin and Richart [43]), and the exponents a_{v} and a_{h} are close to 0.5 for subangular sand [8, 9], and to 0.4 for subrounded sand. Kuwano and Jardine [8] concluded that for sands the overconsolidation and recent stress history do not affect the moduli, although these factors strongly influence the extent of the linear response. Hoque and Tatsuoka [9] observe that in triaxial compression and extension tests, at stress ratios $\sigma_{\mathrm{v}}/\sigma_{\mathrm{h}} > 2.5$ and $\sigma_{\mathrm{v}}/\sigma_{\mathrm{h}} < 1/2.5$, respectively, an important *degradation* of the elastic stiffness, occurs. This is consistent with results by Connoly and Kuwano [55] and Kuwano and Jardine [8], who address this 'catastrophic fall' of elastic stiffness to the disruption of the system of particle contacts and force chain assembly due to dilation. This elastic degradation has never been previously modelled.

Experimental evaluations of the anisotropy of elastic shear stiffness are usually obtained by measuring shear wave velocities through bender elements [8],[¶¶] thus obtaining a power law dependency on stress state, similar to that used for Young moduli, namely

$$G_{\mathrm{vh}} = C_{\mathrm{vh}} f(v) \left(\frac{\sigma_{\mathrm{v}}}{p_{\mathrm{r}}}\right)^{a_{\mathrm{vh}}} \left(\frac{\sigma_{\mathrm{h}}}{p_{\mathrm{r}}}\right)^{b_{\mathrm{vh}}}, \quad G_{\mathrm{hv}} = C_{\mathrm{hv}} f(v) \left(\frac{\sigma_{\mathrm{v}}}{p_{\mathrm{r}}}\right)^{a_{\mathrm{hv}}} \left(\frac{\sigma_{\mathrm{h}}}{p_{\mathrm{r}}}\right)^{b_{\mathrm{hv}}} \tag{A3}$$

where $a_{\mathrm{vh}} = 0.32$, $b_{\mathrm{vh}} = 0.20$, $a_{\mathrm{hv}} = -0.04$, $b_{\mathrm{hv}} = 0.53$, for Ham River sand [8].

More recently, Hong Nam and Koseki [49] measured the evolution of elastic stiffness in torsional loading tests performed in a hollow cylinder apparatus, involving a rotation of principal stress axes. Even in this case, a power law dependency of the elastic properties in the direction of principal stress axes *versus* principal stresses has been proposed to interpolate the experimental measurements.

APPENDIX B: GENERAL, PLASTIC-DEPENDENT, NONLINEAR FREE-ENERGY AND COMPLEMENTARY FREE-ENERGY DENSITY FUNCTIONS

A more general expression of the elastic free-energy density than (21) is suggested to be

$$\varphi(\boldsymbol{\varepsilon}_{\mathrm{e}}, \boldsymbol{\varepsilon}_{\mathrm{p}}) = \alpha d(-\mathrm{tr}(\mathbf{B}\boldsymbol{\varepsilon}_{\mathrm{e}}))^n + \beta d\,(-\mathrm{tr}(\mathbf{B}\boldsymbol{\varepsilon}_{\mathrm{e}}))^m\,(\mathrm{tr}(\mathbf{B}\boldsymbol{\varepsilon}_{\mathrm{e}})^2)^l \tag{B1}$$

which reduces to (21) when $m = 0$.

This elastic free energy with $n = 3$, $m = 1$, and $l = 1$ gives simulations that are nearly coincident with those reported in this work.

[¶¶] It is curious that these authors observed that the velocities of propagation V_{vh} and V_{hv} are different when the sample is subject to compression, tangent elastic stiffness tensor loses the major symmetry, and proposed an explanation based on the distribution of grain contacts. This finding has also been substantiated by HongNam & Koseki [49].

DOI: 10.1002/nag

Alternatively, a *different* formulation in terms of complementary free-energy density may be given in the following form:

$$\Psi(\boldsymbol{\sigma}, \boldsymbol{\varepsilon}_{\mathrm{p}}) = \frac{a}{d}\left(-\frac{\mathrm{tr}(\mathbf{B}^{-1}\boldsymbol{\sigma})}{p_{\mathrm{r}}}\right)^{N} + \frac{b}{d}\left(-\frac{\mathrm{tr}(\mathbf{B}^{-1}\boldsymbol{\sigma})}{p_{\mathrm{r}}}\right)^{M}\left(\frac{\mathrm{tr}(\mathbf{B}^{-1}\boldsymbol{\sigma})^{2}}{p_{\mathrm{r}}^{2}}\right)^{L} \tag{B2}$$

where a, b, L, M, and N are material parameters, $p_{\mathrm{r}} = 1\,\mathrm{kPa}$ is a reference pressure, and d governs degradation and void-ratio dependency. Note that *the two formulations* (B1) *and* (B2) *are not identical, but provide close results for* $N = 1.5$, $M = 0$, *and* $L = 0.75$ *and for* $N = 1.5$, $M = -0.5$, *and* $L = 1$.

APPENDIX C: AN ALGEBRAIC FORM FOR TENSORIAL PRODUCTS (27)

Taking into account the relationship existing between symmetric second-order tensors, fourth-order tensors having minor symmetries and vectors of dimension 6, and 6×6 matrices, respectively, the following vectorial representation can be given to every second-order symmetric tensor $\mathbf{C}$:

$$[C_{11},\ C_{22},\ C_{33},\ \sqrt{2}C_{12},\ \sqrt{2}C_{13},\ \sqrt{2}C_{23}]^{\mathrm{T}}$$

so that the fourth-order tensor $\mathbf{A} \otimes \mathbf{B}$ can be represented as

$$\begin{bmatrix}
A_{11}B_{11} & A_{11}B_{22} & A_{11}B_{33} & \sqrt{2}A_{11}B_{12} & \sqrt{2}A_{11}B_{13} & \sqrt{2}A_{11}B_{23} \\
A_{22}B_{11} & A_{22}B_{22} & A_{22}B_{33} & \sqrt{2}A_{22}B_{12} & \sqrt{2}A_{22}B_{13} & \sqrt{2}A_{22}B_{23} \\
A_{33}B_{11} & A_{33}B_{22} & A_{33}B_{33} & \sqrt{2}A_{33}B_{12} & \sqrt{2}A_{33}B_{13} & \sqrt{2}A_{33}B_{23} \\
\sqrt{2}A_{12}B_{11} & \sqrt{2}A_{12}B_{22} & \sqrt{2}A_{12}B_{33} & 2A_{12}B_{12} & 2A_{12}B_{13} & 2A_{12}B_{23} \\
\sqrt{2}A_{13}B_{11} & \sqrt{2}A_{13}B_{22} & \sqrt{2}A_{13}B_{33} & 2A_{13}B_{12} & 2A_{13}B_{13} & 2A_{13}B_{23} \\
\sqrt{2}A_{23}B_{11} & \sqrt{2}A_{23}B_{22} & \sqrt{2}A_{23}B_{33} & 2A_{23}B_{12} & 2A_{23}B_{13} & 2A_{23}B_{23}
\end{bmatrix}$$

the fourth-order tensor $\mathbf{B}\underline{\otimes}\mathbf{B}$ as (only the upper half of the symmetric 6×6 matrix is given)

$$\begin{bmatrix}
B_{11}^2 & B_{12}^2 & B_{13}^2 & \sqrt{2}B_{11}B_{12} & \sqrt{2}B_{11}B_{13} & \sqrt{2}B_{12}B_{13} \\
 & B_{22}^2 & B_{23}^2 & \sqrt{2}B_{22}B_{12} & \sqrt{2}B_{12}B_{23} & \sqrt{2}B_{22}B_{23} \\
 & & B_{33}^2 & \sqrt{2}B_{13}B_{23} & \sqrt{2}B_{33}B_{13} & \sqrt{2}B_{33}B_{23} \\
 & & & (B_{11}B_{22} + B_{12}^2) & (B_{11}B_{23} + B_{12}B_{13}) & (B_{12}B_{23} + B_{22}B_{13}) \\
 & & & & (B_{11}B_{33} + B_{13}^2) & (B_{12}B_{33} + B_{13}B_{23}) \\
 & & & & & (B_{22}B_{33} + B_{23}^2)
\end{bmatrix}$$

DOI: 10.1002/nag

and the fourth-order tensor $\mathbf{B}\overline{\otimes}\mathbf{I} + \mathbf{I}\overline{\otimes}\mathbf{B}$ as (only the upper half of the symmetric 6×6 matrix is given)

$$\begin{bmatrix} 2B_{11} & 0 & 0 & \sqrt{2}B_{12} & \sqrt{2}B_{13} & 0 \\ & 2B_{22} & 0 & 0 & 0 & \sqrt{2}B_{23} \\ & & 2B_{33} & 0 & \sqrt{2}B_{31} & \sqrt{2}B_{32} \\ & & & (B_{11}+B_{22}) & B_{23} & B_{13} \\ & & & & (B_{11}+B_{33}) & B_{12} \\ & & & & & (B_{22}+B_{33}) \end{bmatrix}$$

APPENDIX D: COEFFICIENTS k_i, $\tilde{k}_i$ AND $\bar{k}_i$

The complete expressions for the coefficients k_i, $\tilde{k}_i$, and $\bar{k}_i$ appearing in Equations (26)–(29) are listed below.

$$k_1 = \alpha d n (n-1)(-\mathrm{tr}(\mathbf{B}\boldsymbol{\varepsilon}_\mathrm{e}))^{n-2} \tag{D1}$$

$$k_2 = 2\beta d l (l-1)(\mathrm{tr}(\mathbf{B}\boldsymbol{\varepsilon}_\mathrm{e})^2)^{l-2} \tag{D2}$$

$$k_3 = 2\beta d l (\mathrm{tr}(\mathbf{B}\boldsymbol{\varepsilon}_\mathrm{e})^2)^{l-1} \tag{D3}$$

$$\tilde{k}_1 = \alpha d n (n-1)(-\mathrm{tr}(\mathbf{B}\boldsymbol{\varepsilon}_\mathrm{e}))^{n-2} \tag{D4}$$

$$\tilde{k}_2 = -\alpha d n (-\mathrm{tr}(\mathbf{B}\boldsymbol{\varepsilon}_\mathrm{e}))^{n-1} \tag{D5}$$

$$\tilde{k}_3 = 4\beta d l (l-1)(\mathrm{tr}(\mathbf{B}\boldsymbol{\varepsilon}_\mathrm{e})^2)^{l-2} \tag{D6}$$

$$\tilde{k}_4 = 2\beta d l (\mathrm{tr}(\mathbf{B}\boldsymbol{\varepsilon}_\mathrm{e})^2)^{l-1} \tag{D7}$$

$$\bar{k}_1 = -\alpha n (-\mathrm{tr}(\mathbf{B}\boldsymbol{\varepsilon}_\mathrm{e}))^{n-1} \tag{D8}$$

$$\bar{k}_2 = 2\beta l (\mathrm{tr}(\mathbf{B}\boldsymbol{\varepsilon}_\mathrm{e})^2)^{l-1} \tag{D9}$$

APPENDIX E: SUFFICIENT CONDITIONS FOR POSITIVE DEFINITENESS OF THE TANGENT STIFFNESS TENSOR $\mathbb{D}$, EQUATIONS (30)

The condition of positive definiteness of fourth-order tensor $\mathbb{D}$ given by Equation (26) can be written as

$$\mathbf{X} \cdot \mathbb{D}[\mathbf{X}] = k_1(\mathbf{B}\cdot\mathbf{X})^2 + k_3 \mathbf{X}\cdot\mathbf{B}\mathbf{X}\mathbf{B} + k_2(\mathbf{B}\boldsymbol{\varepsilon}_\mathrm{e}\mathbf{B}\cdot\mathbf{X})^2 > 0 \quad \forall \mathbf{X}, \boldsymbol{\varepsilon}_\mathrm{e} \in \mathrm{Sym} \tag{E1}$$

Employing now the expedient introduced by Bigoni and Loret [33] of defining

$$\tilde{\mathbf{X}} = \mathbf{B}^{1/2}\mathbf{X}\mathbf{B}^{1/2}, \quad \tilde{\boldsymbol{\varepsilon}}_\mathrm{e} = \mathbf{B}^{1/2}\boldsymbol{\varepsilon}_\mathrm{e}\mathbf{B}^{1/2} \tag{E2}$$

DOI: 10.1002/nag

where $\mathbf{B}^{1/2}$ is the square root of tensor $\mathbf{B}$, defined in such a way that $\mathbf{B}^{1/2}\mathbf{B}^{1/2}=\mathbf{B}$, condition (E1) becomes

$$\mathbf{X}\cdot\mathbb{D}[\mathbf{X}]=k_1(\operatorname{tr}\tilde{\mathbf{X}})^2+k_3\tilde{\mathbf{X}}\cdot\tilde{\mathbf{X}}+k_2(\tilde{\boldsymbol{\varepsilon}}_e\cdot\tilde{\mathbf{X}})^2>0\quad\forall\tilde{\mathbf{X}},\tilde{\boldsymbol{\varepsilon}}_e\in\mathrm{Sym}\tag{E3}$$

Note that the tensors $\tilde{\mathbf{X}}$ and $\tilde{\boldsymbol{\varepsilon}}_e$ are completely generic, since $\mathbf{X}$ and $\boldsymbol{\varepsilon}_e$ are arbitrary.

Now, the proof that conditions (30) are sufficient for positive definiteness of $\mathbb{D}$ for every elastic deformation $\boldsymbol{\varepsilon}_e$ is obtained from the following.

- For every purely deviatoric tensors $\tilde{\mathbf{X}}$ (i.e. $\operatorname{tr}\tilde{\mathbf{X}}=0$), condition (E3) becomes

$$\mathbf{X}\cdot\mathbb{D}[\mathbf{X}]=k_3\tilde{\mathbf{X}}\cdot\tilde{\mathbf{X}}+k_2(\tilde{\boldsymbol{\varepsilon}}_e\cdot\tilde{\mathbf{X}})^2>0\tag{E4}$$

  which is satisfied for every $\tilde{\boldsymbol{\varepsilon}}_e$ if and only if conditions $(30)_2$ and $(30)_3$ are satisfied.
- For a generic tensor $\tilde{\mathbf{X}}$, using the Cauchy–Schwarz inequality

$$(\operatorname{tr}\tilde{\mathbf{X}})^2\leqslant 3(\tilde{\mathbf{X}}\cdot\tilde{\mathbf{X}})\tag{E5}$$

  we obtain

$$\mathbf{X}\cdot\mathbb{D}[\mathbf{X}]\geqslant\left(k_1+\frac{1}{3}k_3\right)(\operatorname{tr}\tilde{\mathbf{X}})^2+k_2(\tilde{\boldsymbol{\varepsilon}}_e\cdot\tilde{\mathbf{X}})^2\quad\forall\tilde{\mathbf{X}},\tilde{\boldsymbol{\varepsilon}}_e\in\mathrm{Sym}\tag{E6}$$

  revealing that, excluding purely deviatoric tensors $\tilde{\mathbf{X}}$ (i.e. for $\operatorname{tr}\tilde{\mathbf{X}}\neq 0$), conditions $(30)_1$ and $(30)_3$ are sufficient for positive definiteness of $\mathbb{D}$ (for every $\tilde{\boldsymbol{\varepsilon}}_e$).

It is not difficult to prove that conditions (30) become also necessary for positive definiteness of $\mathbb{D}$ (for every $\tilde{\boldsymbol{\varepsilon}}_e$) when coefficients k_i, $i=1,\ldots,3$ are constant.

APPENDIX F: SIMULATION OF TYPICAL LABORATORY TESTS AT SUBSTANTIAL STRAIN

In order to highlight the characteristics of the different nonlinear elasticity models, simulations of some typical laboratory tests are given in the following. In particular, drained triaxial tests, drained biaxial tests, and undrained triaxial tests are considered, to analyse tests in which an increasing constraint in some components of the total strain is involved. Figure F1 shows the comparison of simulated and measured drained triaxial compression tests performed at the same confining pressure on samples broadly ranging in density, $e_0=\{0.574, 0.945\}$. Since the LEA model gives results practically coincident with the NLEA model, only the latter is shown. Moreover, the simulations obtained with the linear, isotropic LEI model are also included for comparison. Although the increase in the initial stiffness passing from the LEI to the NLEA-D is evident, it may be concluded that in the simulations of drained triaxial tests the effects of elastic stiffness are fairly small, particularly at large strain.

The constitutive parameters describing the irreversible behaviour (Table II) have been kept almost constant, in order to highlight the effects induced by the elasticity model. Consequently, some details of the simulations, e.g. the volumetric response of NLEA-D model, might be improved by adjusting the constitutive parameters of Table II.

DOI: 10.1002/nag

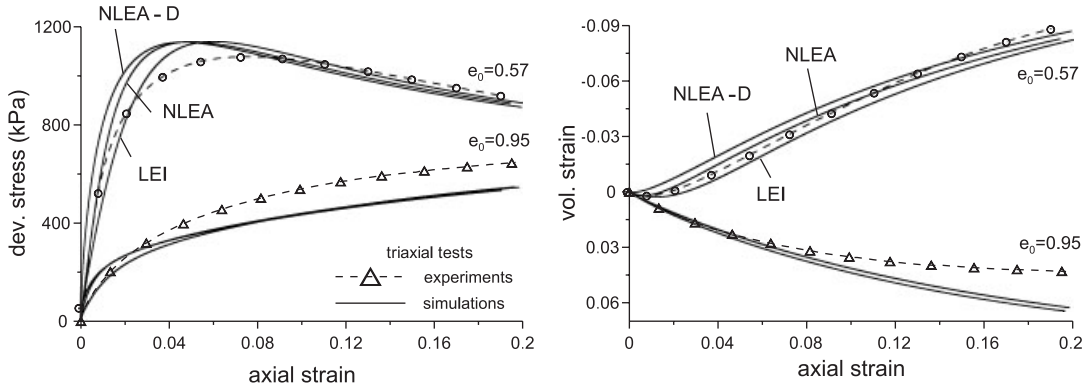

Figure F1. Comparison between simulations and experiments: effects of the initial density on drained, conventional triaxial compression tests, with the same initial pressure, $p_0 = 300$ kPa, for Hostun sand RF. Deviatoric stress *versus* axial strain (left), volumetric *versus* axial strain (right).

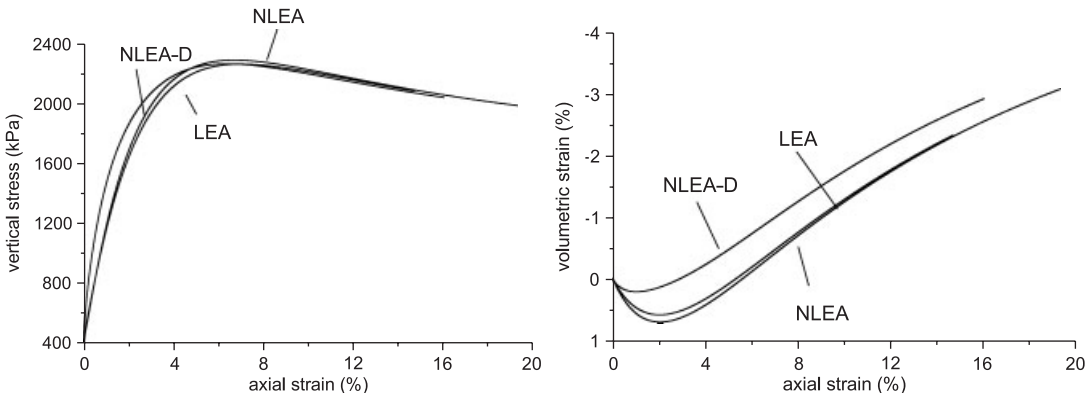

Figure F2. Simulation of drained, biaxial compression tests, with the same initial pressure, $p_0 = 400$ kPa, for dense Hostun sand RF ($e_0 = 0.673$). Vertical stress *versus* axial strain (left), volumetric *versus* axial strain (right).

The simulated drained biaxial compression tests performed at a confining pressure of 400 kPa on a dense Hostun sand sample ($e_0 = 0.673$) is shown in Figure F2. In this case, the constraint of null out-of-plane strain makes the effects of the elasticity models slightly more important, particularly in the volumetric response.

Finally, the effects of the elasticity model on the simulations of undrained triaxial compression tests on loose Hostun sand are shown in Figure F3, together with experimental results. Since the simulations of the LEA model are very similar to those of the NLEA model, only results obtained with the latter model have been reported in Figure F3. Due to the constraint of null total volumetric strain, the effects of the elasticity are important. In particular, it appears from the comparison of NLEA and NLEA-D models that the value of elastic stiffness and its degradation properties play a key role. Note in addition that a very high elastic stiffness makes the simulations very sensitive to experimental imperfections (membrane penetration in undrained tests and grain penetration into

DOI: 10.1002/nag

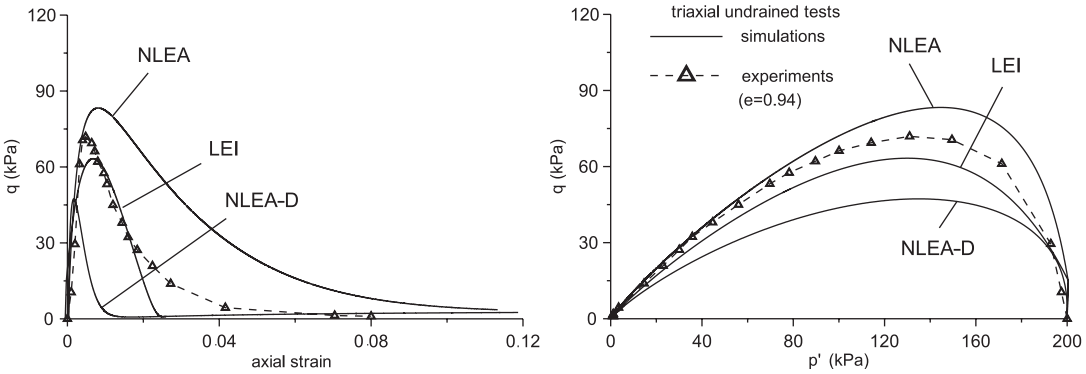

Figure F3. Comparison between simulations and experiments: effects of the elasticity model on undrained, conventional triaxial compression tests, at initial pressure, $p_0 = 200$ kPa, for loose Hostun sand RF ($e_0 = 94$). Deviatoric stress *q versus* axial strain (left), effective stress path in q–p plane (right).

the membrane in the out-of-plane direction of biaxial tests), which have not been considered in the results shown in Figure F3.

ACKNOWLEDGEMENTS

Financial support of MURST-Cofin 2005, prot. 2005085973_002 (D.B.) is gratefully acknowledged.

REFERENCES

1. Jardine RJ, Symes MJ, Burland JB. The measurement of soil stiffness in the triaxial apparatus. *Géotechnique* 1984; **34**:323–340.
2. Seed HB, Wong RT, Idriss IM, Tokimatsu K. Moduli and damping factors for dynamic analyses of cohesionless soils. *Journal of Geotechnical Engineering Division* (ASCE) 1986; **105**:871–880.
3. Burland JB. Ninth Laurits Bjerrum Memorial Lecture: small is beautiful—the stiffness of soils at small strains. *Canadian Geotechnical Journal* 1989; **26**:499–516.
4. Jamiolkowski M, Leuroeuil S, Lo Presti DCF. Design parameters from theory to practice. *Geo.coast '91 International Conference*, Yokohama, vol. 2, 1991; 877–917.
5. Tatsuoka F, Shibuya S. Deformation characteristics of soils and rocks from field and laboratory tests. Keynote lecture. *Ninth ACSMFE*, Bangkok, vol. 2, 1991; 101–170.
6. Atkinson JH, Sallfors G. Experimental determination of soil properties (stress-strain-time). *General Report 10th ECSMFE*, Florence, Balkema, vol. 3, 1991; 915–958.
7. Burghignoli A, Pane V, Cavalera L, Sagaseta C, Cuellar V, Pator M. Modelling stress–strain–time behaviour of natural soils. *General Report 10th ECSMFE*, Florence, Balkema, vol. 3, 1991; 959–979.
8. Kuwano R, Jardine RJ. On the applicability of cross-anisotropic elasticity to granular materials at very small strains. *Géotechnique* 2002; **52**:727–749.
9. Hoque E, Tatsuoka F. Effects of stress ratio on small-strain stiffness during triaxial shearing. *Géotechnique* 2004; **54**:429–439.
10. Gazetas G. Stress and displacement in cross-anisotropic soils. *Journal of the Geotechnical Engineering Division* (ASCE) 1982; **108**:532–553.
11. Kirkpatrick WM, Rennie IA. Directional properties of consolidated caolin. *Géotechnique* 1972; **22**:166–169.
12. Ward WH, Samuels SG, Gutler ME. Further studies of the properties of London clay. *Géotechnique* 1959; **9**:321–344.
13. Atkinson JH. Anisotropic elastic deformations in laboratory tests on undisturbed London clay. *Géotechnique* 1975; **25**:357–384.

DOI: 10.1002/nag

14. Hoque E, Tatsuoka F. Anisotropy in elastic deformation of granular materials. *Soils and Foundation* 1998; **38**(2):163–179.
15. Atkinson JH. Non-linear soil stiffness in routine design. *Géotechnique* 2000; **50**:487–508.
16. Zytynski M, Randolph MF, Nova R, Wroth CP. On modelling the unloading–reloading behaviour of soils. *International Journal for Numerical and Analytical Methods in Geomechanics* 1978; **2**:87–93.
17. Vermeer PA. A double hardening model for sand. *Géotechnique* 1978; **28**:413–433.
18. Boyce HR. A non-linear model for the elastic behaviour of granular materials under repeated loading. In *Proceedings of the International Symposium on Soils under Cyclic and Transient Loading*, Swansea, U.K., 1980; 285–294.
19. Mroz Z, Norris VA. Elastoplastic and viscoplastic constitutive models for soils. *Soil Mechanics—Transient and Cyclic Loading*. Wiley: New York, 1982.
20. Loret B. On the choice of elastic parameters for sand. *International Journal for Numerical and Analytical Methods in Geomechanics* 1985; **9**:285–292.
21. Houlsby GT. The use of a variable shear modulus in elastic–plastic models for clays. *Computers and Geotechnics* 1985; **1**:3–13.
22. Jardine RJ, Potts DM, Fourie AB, Burland JB. Studies of the influence of non-linear stress–strain characteristics in soil–structure interaction. *Géotechnique* 1986; **36**:377–396.
23. Lade PV, Nelson RB. Modelling the elastic behaviour of granular materials. *International Journal for Numerical and Analytical Methods in Geomechanics* 1987; **11**:521–542.
24. Molenkamp F. A simple model for isotropic non-linear elasticity of frictional materials. *International Journal for Numerical and Analytical Methods in Geomechanics* 1988; **12**:467–475.
25. Puzrin AM, Burland JB. Non-linear model of small-strain behaviour of soils. *Géotechnique* 1998; **48**:217–233.
26. Houlsby GT, Amorosi A, Rojas E. Elastic moduli of soils, dependent on pressure: a hyperelastic formulation. *Géotechnique* 2005; **55**:383–392.
27. Hueckel T, Tutumluer E, Pellegrini R. A note on non-linear elasticity of isotropic overconsolidated clays. *International Journal for Numerical and Analytical Methods in Geomechanics* 1992; **16**:603–618.
28. Walton K. The effective elastic moduli of a random packing of spheres. *Journal of the Mechanics and Physics of Solids* 1987; **35**:213–226.
29. Goddard JD. Nonlinear elasticity and pressure-dependent wave speeds in granular media. *Proceedings of the Royal Society of London*, *Series A* 1990; **430**:105–131.
30. Hueckel T. On plastic flow of granular and rock-like materials with variable elasticity moduli. *Bulletin of the Polish Academy of Sciences*, *Engineering Sciences Series* 1975; **23**:405–414.
31. Hueckel T. Coupling of elastic and plastic deformation of bulk solids. *Meccanica* 1976; **11**:227–235.
32. Hueckel T, Maier G. Incremental boundary value problems in the presence of coupling of elastic and plastic deformations: a rock mechanics oriented theory. *International Journal of Solids Structures* 1977; **13**:1–15.
33. Maier G, Hueckel T. Nonassociated and coupled flow-rules of elastoplasticity for rock-like materials. *International Journal of Rock Mechanics and Mining Science* 1979; **16**:77–92.
34. Valanis KC. A theory of damage in brittle materials. *Engineering Fracture Mechanics* 1990; **36**:403–416.
35. Bigoni D, Loret B. Effects of elastic anisotropy on strain localization and flutter instability in plastic solids. *Journal of the Mechanics and Physics of Solids* 1999; **47**:1409–1436.
36. Stokoe II KH, Hwang SK, Lee JNK, Andrus RD. Effects of various parameters on the stiffness and damping of soils at small to medium strains. *Proceedings of the 1st International Symposium on Pre-failure Deformation of Geomaterials*, Sapporo, vol. 2, 1995; 785–816.
37. Lo Presti DCF, Pallara O, Lancellotta R, Armandi M, Maniscalco R. Monotonic and cyclic behaviours of two sands at small strains. *Geotechnical Testing Journal* 1993; **16**:409–424.
38. Hill R, Rice JR. Elastic potentials and the structure of inelastic constitutive laws. *SIAM Journal on Applied Mathematics* 1973; **25**:448–461.
39. Bigoni D. Bifurcation and instability of nonassociative elasticplastic solids. In *Material Instabilities in Elastic and Plastic Solids*, CISM Lecture Notes No. 414, Petryk H (ed.). Springer: Wien, New York, 2000; 1–52.
40. Zysset PK, Curnier A. An alternative model for anisotropic elasticity based on fabric tensors. *Mechanics of Materials* 1995; **21**:243–250.
41. Gajo A, Bigoni D, Muir Wood D. Multiple shear band development and related instabilities in granular materials. *Journal of the Mechanics and Physics of Solids* 2004; **52**:2683–2724.
42. Lings ML, Pennington DS, Nash DFT. Anisotropic stiffness parameters and their measurement in a stiff natural clay. *Géotechnique* 2000; **50**:109–125.

DOI: 10.1002/nag

43. Hardin BO, Richart FE. Elastic wave velocities in granular soils. *Journal of Soil Mechanics and Foundation Division* (ASCE) 1963; **89**:33–65.
44. Gajo A, Muir Wood D. A kinematic hardening constitutive model for sands: the multiaxial formulation. *International Journal for Numerical and Analytical Methods in Geomechanics* 1999; **23**:925–965.
45. Gajo A, Muir Wood D. Severn-trent sand: a kinematic hardening constitutive model for sands: the $q-p$ formulation. *Géotechnique* 1999; **49**:595–614.
46. Been K, Jefferies MJ. A state parameter for sands. *Géotechnique* 1985; **35**:99–112.
47. Argyris JH, Faust G, Szimmat J, Warnke P, Willam K. Recent developments in the finite element analysis of prestressed concrete reactor vessels. *Nuclear Engineering and Design* 1974; **28**:42–75.
48. Lancellotta R, Calavera J. *Fondazioni*. McGraw-Hill: London, 1999.
49. HongNam N, Koseki J. Quasi-elastic deformation properties of Toyura sand in cyclic triaxial and torsional loadings. *Soils and Foundation* 2005; **45**(5):19–38.
50. Gajo A, Muir Wood D, Bigoni D. On certain critical material and testing characteristics affecting shear band development in sand. *Géotechnique* 2007; **57**:449–461.
51. Stokoe II KH, Lee JNK, Lee SHH. Characterization of soil in calibration chambers with seismic waves. *Proceedings of ISOCCTI*, Clekson, NY, vol. 2, 1991; 363–376.
52. Bellotti R, Jamiolkowski M, Lo Presti DCF, O'Neill DA. Anisotropy of small strain stiffness in Ticino sand. *Géotechnique* 1996; **46**:115–131.
53. Hardin BO. The nature of stress–strain behavior for soils. *Specialty Conference on Earthquake Engineering and Soil Dynamics*, Pasadena, CA, *Proceedings of the ACSE Geotechnical Division*, New York, vol. 1, 1978; 3–90.
54. Hardin BO, Bladford GE. Elasticity of particulate materials. *Journal of Geotechnical Engineering* (ASCE) 1989; **89**:788–805.
55. Connoly TM, Kuwano R. The measurement of $G_{\max}$ in a resonant column, bender element, torsional shear apparatus. In *Proceedings of the 2nd International Symposium Pre-failure Deformation Characteristics of Geomaterials*, Torino, vol. 1, 1999; 73–81.

DOI: 10.1002/nag